Programmed “disarming” of the neutrophil proteome reduces the magnitude of inflammation

José M. Adrover[1], Alejandra Aroca-Crevillén[1], Georgiana Crainiciuc[1], Fernando Ostos[2], Yeny Rojas-Vega[3], Andrea Rubio-Ponce[1], Catia Cilloniz[4], Elena Bonzón-Kulichenko[5], Enrique Calvo[5], Daniel Rico[6], María A. Moro[2], Christian Weber[7,8], Ignacio Lizasoaín[2], Antoni Torres[4], Jesús Ruiz-Cabello[3,9], Jesús Vázquez[5] and Andrés Hidalgo[1,7]

[1] Area of Cell and Developmental Biology, Fundación Centro Nacional de Investigaciones Cardiovasculares, 28029 Madrid, Spain
[2] Unidad de Investigación Neurovascular, Department of Pharmacology, Faculty of Medicine, Universidad Complutense and Instituto de Investigación Hospital 12 de Octubre (i+12), Madrid, Spain
[3] Advanced Imaging Unit, Fundación Centro Nacional de Investigaciones Cardiovasculares, 28029 Madrid, Spain
[4] Department of Pneumology, Institut Clinic de Respiratori, Hospital Clinic of Barcelona, and Institut d’Investigacions Biomèdiques August Pi i Sunyer (IDIBAPS), University of Barcelona, Ciber de Enfermedades, Barcelona, Spain
[5] Cardiovascular Proteomics Laboratory, Centro Nacional de Investigaciones Cardiovasculares Carlos III (CNIC), Madrid, Spain; and Centro de Investigación Biomédica en Red de Enfermedades Cardiovasculares (CIBERCV), Madrid, Spain
[6] Institute of Cellular Medicine, Newcastle University, Framlington Place, Newcastle upon Tyne NE2 4HH, UK
[7] Institute for Cardiovascular Prevention, Ludwig Maximillians University, Munich, Germany
[8] German Cardiovascular Research Centre (DZHK), partner site Munich Heart Alliance, Munich, Germany and Dept. Biochemistry, Cardiovascular Research Institute Maastricht (CARIM), Maastricht, The Netherlands.
[9] CIC biomaGUNE, 2014, Donostia-San Sebastián, Spain; IKERBASQUE, Basque Foundation for Science, Spain; Ciber de Enfermedades Respiratorias (CIBERES), Madrid, Spain; and Universidad Complutense Madrid, Madrid, Spain.

Correspondence: Andres Hidalgo (ahidalgo@cnic.es)

Abstract

The anti-microbial functions of neutrophils are facilitated by a defensive armamentarium of proteins stored in granules, and by the formation of neutrophil extracellular traps (NETs). The toxic nature of both structures, however, poses a threat to highly vascularized tissues, such as the lungs, in which neutrophils marginate. Here, we identify a cell-intrinsic program that naturally modifies the neutrophil proteome in the circulation, causing progressive loss of granule content and NET-forming capacity. This programmed behavior was driven by the receptor CXCR2 and disappeared in the absence of regulators of circadian time. As a consequence, lungs were protected from inflammatory injury at diurnal times or in mouse mutants in which granule content was low. Changes in the proteome, granule content and NET formation also occurred in human neutrophils, and correlated with the incidence and severity of respiratory distress in pneumonia patients. Our findings unveil a "disarming" strategy of neutrophils that depletes protein stores to reduce the magnitude of inflammation.

Introduction

The foremost role of neutrophils is to protect the host from microbial infections. To carry out their protective functions, neutrophils are endowed with a number of highly specialized features. Most prominent among these is the accumulation inside cytoplasmic granules of receptors, proteases, antimicrobial peptides and proteins needed for the production of reactive oxygen species (ROS) or DNA-based extracellular traps (NETs), which combined are highly toxic and allow for effective encounter and containment of pathogens [1, 2]. Several types of granules coexist in the neutrophil cytoplasm [3], including primary (azurophilic) granules that contain large amounts of myeloperoxidase (MPO), as well as secondary (specific), tertiary (gelatinase) granules and secretory vesicles, each of which carries distinct types of cargo [1, 4]. The different neutrophil granules are formed at different stages of granulopoiesis in the bone marrow [5, 6], and the synthesis of granule proteins markedly declines as neutrophils complete their differentiation [7, 8]. This medullary-restricted synthesis of anti-microbial proteins contrasts with the preferred synthesis of receptors needed for sensing, migration and phagocytosis once neutrophils mature and reach the circulation [7, 8]. Thus, neutrophils gate the synthesis of a basic stock of toxic granule proteins during early stages of maturation inside the bone marrow, thereby generating an armamentarium ready for deployment once they sense danger in the periphery.

A second prominent feature of neutrophils is a short lifetime in the circulation, which is generally estimated to be 6 to 10 hours at least in mice [9, 10], and is followed by rapid clearance from blood into tissues [11, 12]. However, disappearance from blood does not imply immediate elimination, and cleared neutrophils infiltrate or marginate in multiple organs, with a preference for the spleen, bone marrow and the lungs [11]. While the physiological purpose of migration of neutrophils into naïve tissues remains unclear, we have shown that this process is enabled by a cell-intrinsic program (referred to as *aging*[13]) that relies on the receptor CXCR2 and the core clock protein Bmal1[14]. These defining features of neutrophils, namely storage of cytotoxic proteins in granules, short lifetimes and clearance into tissues, are paradoxical because they could generate potential threats to highly vascularized tissues, such as the lungs, in which neutrophils marginate at specific times of day (night in mice [11]). In keeping with these observations, the lungs are highly susceptible to neutrophil-mediated damage resulting in respiratory dysfunction and death, as demonstrated in murine models of endotoxin- or antibody-induced lung injury [15-17]. Consistent with the findings in mice, neutrophil-mediated acute vascular damage followed by pulmonary edema and distress is common in patients with underlying pneumococcal infections or other pre-existing conditions [15, 18].

Puzzled by the co-existence of these potentially harmful features in circulating neutrophils, we predicted that unknown mechanisms might prepare neutrophils such that they became less toxic to host tissues into which they emigrated from blood. By combining proteomic, imaging and various genetic mouse models, we discovered that the neutrophil proteome naturally “disarms”, such that neutrophils lose granule content during their lifetime in circulation. We find that the process is cell-autonomous, relies on Bmal1 and CXCR2 signaling, and results in blunted capacity to produce NETs, altogether rendering neutrophils less toxic before they reach tissues. We show that this process effectively protected the lungs from inflammatory injury in mice, and that human neutrophils undergo similar proteomic alterations that correlated with diurnal protection from pulmonary injury in pneumonia patients. Overall, our results uncover a proteomic program in neutrophils that anticipates their natural migration into tissues, thus protecting the host from their cytotoxic activity.

Results

Diurnal changes in the neutrophil proteome

Previous studies have shown that neutrophils undergo transcriptional changes while in the circulation [14]. Because transcriptional programs typically take relatively longer times (in the range of hours) and, in the case of neutrophils, the diurnal transcriptional program favors rather than prevents their migration into tissues, we deemed transcriptional regulation unlikely to account for protection of tissues against the toxic activity of neutrophils. We therefore undertook a proteomic approach to explore changes in protein content during the lifetime of neutrophils in the circulation, i.e. at different times after release from the bone marrow. Given the low number of neutrophils that can be purified from the blood of naïve mice at night (when they are freshly released from the marrow) or at noon (when they have spent several hours in circulation)[19], we enriched mice for freshly-released neutrophils by a single injection of a CXCR4 antagonist (AMD3100) which induces rapid mobilization from the marrow [20], and for aged neutrophils by blocking P- and E-selectins with antibodies [14, 19] (**Figure 1a**). The proteomic analysis of both populations yielded 6677 total proteins (**Supplementary Table 1**), of which 171 were differentially enriched in either subset, including regulators of the cytoskeleton (Arghdib, Rufy3) and adhesion proteins (Thbs1, Itgam), as well as components of the Inflammasome (Nlrp3, Nlrp4e), or proteins involved in vesicular transport (Vps33b; **Figure 1b**). We could validate the differential presence of several of the identified proteins by flow cytometry (**Supplementary Fig.1a**), and gene ontology analyses (see **Supplementary Table 2**) revealed a general involvement of the differentially expressed proteins in immune defense, cytokine signaling and angiogenesis (**Supplementary Fig.1b**). The analyses also identified a number of relevant pathways associated with expected functions of neutrophils that had spent different time in the circulation (**Figure 1c**): for example, freshly-released neutrophils were enriched for c-Kit signaling and platelet production pathways, both of which may be reminiscent of their time in the marrow microenvironment, as well as Rho GTPase signaling which agrees with the superior migratory capacity reported for younger neutrophils [14]. Aged neutrophils, in contrast, showed upregulation of protein synthesis, pathogen sensing and respiration, hinting to specialization for effector functions in tissues and enhanced TLR signaling, in agreement with previous reports [14, 21]. Interestingly, comparison of our proteome dataset with transcriptional changes associated with neutrophil aging in blood (data from [14]) revealed poor correlation (**Supplementary Fig. 1c**), suggesting that at least part of the proteomic changes are not driven by direct transcriptional regulation.

Degranulation of circulating neutrophils in the steady-state

Close inspection of the proteomic data revealed that several of the differentially identified proteins corresponded to those stored inside granules (**Supplementary Table 3**). Specifically, we found that proteins stored in different types of granules (azurophilic, specific and tertiary/gelatinase) were enriched in neutrophils newly released from the bone marrow (**Figure 1d**), indicating their progressive loss over time in circulation. Only proteins associated with secretory vesicles were maintained or even enriched in progressively aged (day-associated) neutrophils (**Figure 1d**). Consistent with this, degranulation was a regulated process in the Reactome database (**Supplementary Fig.2a**), further suggesting that circulating neutrophils might be losing granules over time, even under steady-state conditions. Of note, we found similar enrichment in granule proteins when comparing the proteome of AMD3100-mobilized neutrophils with that of circulating neutrophils at ZT5 (**Supplementary Fig.1d-e** and **Supplementary Table 4**), which have spent several hours in the circulation[14, 19].

Cytometric analysis at different times of day showed circadian oscillations in the side-scatter properties of circulating neutrophils, a feature that reflects cell granularity (**Supplementary Fig.2b**). To formally assess if these findings were caused by actual degranulation of neutrophils in blood, we sort-purified neutrophils at multiple times of day and stained for MPO, one of the most abundant proteins stored in azurophilic granules, and analyzed images by high-resolution confocal microscopy (**Figure 1e**). In line with the proteome analyses, we found marked and progressive loss of granules positive for MPO in the neutrophils' cytoplasm, with maximal abundance at zeitgeber time 17 (ZT17; or 17 hours after lights on) and a trough at ZT1 (**Figure 1f**), which correspond to times when freshly marrow-released or aged neutrophils predominate in the circulation, respectively (**Supplementary Fig.2c** and [11, 14, 19]). Remarkably, the diurnal fluctuations in granule content were in anti-phase with the amount of free elastase (a protein from azurophilic granules) activity detectable in plasma (**Figure 1g**), such that peak granule content in cells corresponded with lower elastase activity in plasma, which suggested that at least part of the granules' content was released into the bloodstream. Interestingly, we found that shifts in the light cycle completely re-adjusted the pattern of granule content (**Supplementary Fig.2d)**, indicating that neutrophil degranulation was circadian in nature.

Because circulating neutrophils eventually migrate into tissues or marginate within their vasculature [11], this finding implied that neutrophils within healthy tissues might show features of degranulation. Indeed, examination of neutrophils from lungs, spleen and liver all showed reduced granule content relative to blood and, interestingly, maximal degranulation was

featured by pulmonary neutrophils (**Supplementary Fig.2e-f**) suggesting that this phenomenon might be particularly relevant for this tissue. Altogether, the data provided evidence for homeostatic degranulation of neutrophils in the circulation.

Progressive loss of NET-forming capacity

Besides discharge of granule content, neutrophils exert potent cytotoxic activity through the formation of DNA-based structures containing nuclear- and granule-derived proteins, or neutrophil extracellular traps (NETs) [22]. Notably, proteases stored in azurophilic granules have been shown to degrade the nuclear histones and promote chromatin decondensation during NET formation [23], and granule proteins have been identified in the NET proteome [24]. These studies demonstrated a causal role for granule proteins in NET formation and suggested that granule-rich neutrophils at night might be prone to release NETs. Consistent with this possibility, we found that virtually all of the detected proteins associated with NETs were enriched in the proteome of fresh neutrophils, implying that they were lost as neutrophils aged in blood (**Figure 2a**). To directly examine whether night neutrophils formed NETs more efficiently, we treated neutrophils purified at ZT13 or ZT5 with phorbol myristate acetate (PMA), a strong NET-inducing compound. Confirming our prediction, night neutrophils (ZT13) were more efficient at forming NETs, as identified by the presence of more extracellular DNA decorated with MPO protein and citrullinated Histone 3 (cit-H3; **Figure 2b**), indicating that loss of NET-forming capacity of neutrophils correlates with loss of granule content over time. To confirm this *in vitro* observation in a physiological context, we assessed the presence of NETs in muscles subjected to ischemia-reperfusion, and confirmed the specificity of our staining for NETs in tissues using neutropenic mice ($Lyz2^{Cre}$; $Mcl1^{flox/flox}$; [25]). Consistent with the *in vitro* data, we found numerous NETs scattered in the tissue at ZT13, while few of these structures were detectable at ZT5 (**Figure 2c**).

Altogether, our data suggested that circulating neutrophils undergo proteomic changes and degranulation in the steady-state, with concomitant loss of NET-forming ability. These findings prompted us to query which homeostatic mechanism could underlie a process (degranulation) commonly believed to be elicited upon strong stimulation.

Proteome changes are driven by CXCR2 and the circadian regulator Bmal1

We have previously shown that diurnal changes in neutrophil transcription and migration are driven by a cell-intrinsic clock, whereby expression of *Cxcl2* is regulated diurnally by the molecular clock protein Bmal1 and leads to cell-autonomous, diurnal activation of neutrophils through CXCR2 in the steady-state [14]. To assess whether activation of the same receptor controlled protein content, we first confirmed that treatment with CXCL2 induced degranulation on wild-type neutrophils (**Figure 3a**). Next, to formally test if the CXCL2/CXCR2 axis induced diurnal degranulation of circulating neutrophils *in vivo*, we generated mice with neutrophil-specific deficiency in CXCR2 (*MRP8*^{CRE} *Cxcr2*$^{flox/flox}$; referred to as CXCR2$^{\Delta N}$) [14] and analyzed granule content at ZT13 and ZT5. Compared with wild-type controls, these mice displayed arrhythmicity in granule content (**Figure 3b** and **Supplementary Fig.2b**), and we found a similar loss of diurnal oscillations in mice with global deficiency in CXCL2 (*Cxcl2*$^{-/-}$). Control experiments showed that CXCR2$^{\Delta N}$ neutrophils degranulated in response to PMA and LPS, indicating that impaired diurnal degranulation in the steady-state was not caused by general defects of these cells (**Supplementary Fig.3a-b**). Importantly, and consistent with the notion that granule contents are needed for NET formation, neutrophils from both CXCR2 and CXCL2 mutants also lost diurnal differences in NET formation (ZT5 vs. ZT13; **Figure 3c**), thus demonstrating the involvement of CXCL2/CXCR2 signaling in causing diurnal degranulation. Further, analyses of bone marrow chimeras in which wild-type and *Cxcl2*$^{-/-}$ neutrophils coexisted, revealed higher granule content in *Cxcl2*$^{-/-}$ cells relative to wild-type counterparts, suggesting that CXCL2 produced by neutrophils signals in an autocrine fashion to trigger degranulation (**Figure 3d**).

Because circadian expression of *Cxcl2* is controlled by Bmal1[14], we hypothesized that this transcription factor regulated the diurnal patterns of neutrophil degranulation. Analysis in mice with neutrophil-specific deletion of *Arntl* (which encodes Bmal1; referred to here as Bmal1$^{\Delta N}$ mice) revealed complete absence of circadian degranulation (**Supplementary Fig.4a**) and NET formation relative to wild-type controls (**Supplementary Fig.4b**), suggesting that Bmal1 controlled the changes in the neutrophil proteome. To assess this directly, we performed proteome analysis of neutrophils from Bmal1$^{\Delta N}$ mice purified at day (ZT5) or night-time (ZT13) (**Supplementary Fig.4c**, and **Supplementary Table 5**). In sharp contrast with wild-type cells

(**Figure 1**), Bmal1-deficient neutrophils did not show circadian changes in granule proteins, or in NET-associated proteins (**Supplementary Fig.4d-e**).

Combined, these functional, imaging and proteome analyses are consistent with a model whereby Bmal1 and downstream signaling through CXCL2/CXCR2 cause proteomic changes in neutrophils that result in diurnal loss of cytoplasmic granules, and concomitant loss in the capacity of to form NETs. Because both granules and NETs are important in the pathological activity of neutrophils [26, 27], we next set out to study the consequences of this programmed "disarming" of neutrophils in the context of inflammation.

Diurnal variations in pulmonary protection

To test whether the natural changes in the neutrophil proteome might influence the outcome of inflammatory responses in tissues, we used a model of endotoxin and antibody-induced acute lung inflammation (ALI; [17, 28]). This model is dependent on neutrophils and NETs [29-31], and faithfully recapitulates pulmonary injury that may occur in patients transfused with blood products [32]. Of note, this model of ALI requires a Balb/c genetic background, and we confirmed that this strain underwent diurnal variations in neutrophil number and phenotype (**Supplementary Fig. 5a-c**) similar to those reported in the C57BL/6 strain [14].

Using this model, we detected the presence of NETs in the lungs of Balb/c mice after the induction of ALI by combining staining for MPO, DNA and cit-H3 (**Figure 4a, Movies S1** and **S2**), suggesting involvement of these neutrophil products as previously reported [29, 31]. We next performed high-speed multichannel intravital imaging of the lung microcirculation [33] to gather information not only of the presence of NETs, but also in the kinetics of their *in vivo* formation during ALI. In these analyses, neutrophils were identified by expression of Ly6G and NET-like structures by the rapid extrusion from neutrophils of DNA that was labeled by intravenous injection of Sytox green (**Figure 4b** and **Movie S3**). While in these experiments our setup only allowed for DNA labeling and not for other markers of NETs, the extrusion of such structures was efficiently inhibited in the presence of the PAD4 inhibitor Cl-amidine (**Figure 4c**), suggesting that these represented *bona fide* events of NET release. Continuous tracking of neutrophil behavior in the imaging experiments revealed a more prominent production of these NET-like structures when experiments were performed at night (ZT13; **Figure 4c** and **Movie S3**), which corresponded to the time of increased granule content (**Figure 1e-f**). The enhanced NET production at night was detectable early upon induction of ALI and was sustained over time (**Figure 4c**). In contrast, the number of neutrophils was similar at both times of day or in the

presence of Cl-amidine (**Supplementary Fig.6a** and **6e**). Because platelets have been involved in neutrophil activation and NET formation during ALI [17, 30], we also assessed their possible involvement in the differential response to time of day. We consistently found sharp increases in platelets in pulmonary vessels during ALI, as expected, however their numbers were comparable at both times of day (**Supplementary Fig.6b**), altogether suggesting that the quantity of neutrophils or platelets was not the critical parameter causing diurnal changes in pulmonary inflammation.

To test the consequences of diurnal changes in NET formation in inflamed lungs we next measured the kinetics of edema formation, which is caused by plasma infiltration in the alveolar space. Intravenous Evan's blue injection demonstrated a dramatic increase in pulmonary vascular permeability during ALI, indicating that this model compromised vascular integrity specifically in the lungs but no other tissues (**Supplementary Fig.7a**). We then used computerized tomography (CT) to track the *in vivo* dynamics of this pathological process in mice in which we induced ALI in the morning or at night (**Figure 4d**). We found a rapid and sharp increase in water content that occurred earlier and was strongly enhanced when we induced ALI at night (ZT13; **Figure 4e**), and correlated with reduced survival at this time (**Figure 4f**). Notably, treatment with Cl-amidine protected mice from edema and death, indicating that the release of NETs was a primary cause of ALI (**Figures 4e-f**). These observations suggested that the loss of granule content and capacity to form NETs by neutrophils during the day could provide a mechanism to protect the vasculature from the toxic action of neutrophils.

Pulmonary protection is encoded in neutrophils

Despite the prominent diurnal changes in inflammatory susceptibility to ALI found in wild-type mice, the experiments did not demonstrate a causal relationship between lung inflammation and the neutrophil-intrinsic variations in granule content and NET formation. To assess whether this was the case, we used mice in which neutrophils specifically lacked Bmal1, a transcription factor that induces cell-autonomous expression of CXCL2 thereby promoting diurnal CXCR2 signaling, and CXCR4, a negative regulator of CXCR2 signaling [14]. These models had the advantage over CXCR2$^{\Delta N}$ mice of not compromising the CXCR2-dependent recruitment of neutrophils to the lungs, an important requirement for ALI [34]. Neutrophils from Bmal1$^{\Delta N}$ and CXCR4$^{\Delta N}$ mutant mice have been shown to reproduce the transcriptional and migratory features of night and day neutrophils, respectively [14], and therefore provided an ideal model to assess how programs intrinsic to neutrophils controlled the magnitude of inflammation. Indeed, staining

for MPO+ granules and transmission electron microscopy imaging showed that Bmal1-deficient neutrophils (purified at ZT5) presented elevated number of granules that was similar to wild-type neutrophils at ZT13. In contrast, CXCR4-deficient neutrophils (at ZT5) had strong reductions in granule content, even lower than those found in wild-type neutrophils at ZT5 (**Figure 5a-b**). Consistent with these findings, we found that NET formation in response to PMA was elevated in Bmal1$^{\Delta N}$ neutrophils, and almost completely abrogated in CXCR4$^{\Delta N}$ neutrophils relative to wild-type controls (**Figure 5c**). The findings in these genetic models supported the findings in CXCR2$^{\Delta N}$ mice, indicating that variations in granule content and NET formation were driven by a neutrophil-intrinsic program. Further, they provided a genetic model to test whether the diurnal changes in ALI susceptibility were caused by changes in neutrophil granularity.

We therefore backcrossed the neutrophil-specific deficiencies in Bmal1 and CXCR4 into the ALI-susceptible Balb/c strain, and compared their responses at a single time of day (ZT5), so that only neutrophil-intrinsic properties could drive differences in the inflammatory response. Using intravital microscopy analyses of the lungs after induction of ALI we found rapid and sustained NET formation in Bmal1$^{\Delta N}$ mice, and reductions in CXCR4$^{\Delta N}$ mice that reproduced the differences found in wild-type mice at ZT13 and ZT5, respectively (**Figure 5d**). These differences contrasted with comparable numbers of neutrophils and platelets as well as interactions with each other within the microvasculature of wild type, Bmal1$^{\Delta N}$ and CXCR4$^{\Delta N}$ mice as determined by intravital microscopy and flow cytometry (**Supplementary Fig. 6c-d** and **f-g**), which indicated an otherwise normal behavior of intravascular neutrophils in these mice. In line with the differential formation of NETs, we found strong pulmonary edema and early death in Bmal1$^{\Delta N}$ mice during ALI, while CXCR4$^{\Delta N}$ mice showed remarkable reductions in edema formation and enhanced survival (**Figure 5e-f** and **Movie S4**). Further, the protection seen in CXCR4$^{\Delta N}$ mice correlated with complete preservation of vascular permeability in the lungs after intravenous injection of Evans blue (**Supplementary Fig. 7b-c**). Interestingly, our intravital imaging revealed two modalities of NET ejection that occurred with similar frequencies within inflamed lungs, one in which the extruded NETs were immediately washed away by the bloodstream (“flowing” NETs), and another in which the extruded DNA remained adherent to the vasculature (“adherent” NETs; **Supplementary Fig. 7d** and **Movie S5**). Only the adherent-type NETs were elevated in Bmal1$^{\Delta N}$ mice but not in wild-type or CXCR4$^{\Delta N}$ mice (**Supplementary Fig.7e**), suggesting that the capacity of Bmal1$^{\Delta N}$ neutrophils to directly deposit NETs onto the endothelium might enhance vascular damage.

The distinct phenotype of Bmal1-deficient neutrophils, together with the reported role of Bmal1 in regulating other circadian properties of neutrophils[14] suggested that this might represent an ideal mouse model to directly examine a causal relationship between diurnal proteome changes and diurnal susceptibility to inflammation. Consistent with our proteomic data (**Supplementary Fig.4d-e**), neutrophils from Bmal1$^{\Delta N}$ mice displayed constitutively elevated granule content and capacity to form NETs irrespective of the time of day (**Supplementary Fig. S4a-b**).These altered temporal features paralleled constitutive reduced survival of Bmal1$^{\Delta N}$ mice during ALI, regardless of the time of induction (**Supplementary Fig.8a**). We found a similar loss in circadian granule content and NET formation in neutrophils lacking CXCR4 (**Supplementary Fig.8b-c**), and improved survival of CXCR4$^{\Delta N}$ mutants during ALI that was independent of the time of day (**Supplementary Fig.8a**). These findings in the Bmal1 and CXCR4 mutant mice indicated that impaired diurnal changes in the neutrophil proteome and reduced granule content were causally related to the magnitude of inflammation. Thus, diurnal changes in the neutrophil proteome confers protection against inflammation.

Of note, the number of circulating neutrophils in Bmal1$^{\Delta N}$ mice remained oscillatory and similar to wild-type controls (**Supplementary Fig.8d**), whereas CXCR4$^{\Delta N}$ mutants are neutrophilic[14], indicating that granule content, but not neutrophil numbers, associated with the severity of pulmonary inflammation.

Diurnal changes in the proteome and function of human neutrophils

Clinical manifestations of inflammation have been shown to display circadian oscillations in humans, and to be associated with time-of-day variations in both incidence and severity of cardiovascular disease (CVD; [35-37]). Because neutrophils are associated with many of forms of CVD [27], we hypothesized that a mechanism of neutrophil “disarming” might also be at work in humans and that it could underlie, at least partly, circadian changes in vascular inflammation. We therefore studied a small cohort of healthy volunteers, in which we measured neutrophil counts in blood, and performed proteomic analysis, granule content and NET formation in neutrophils isolated at different times of day (**Figure 6a**). We chose to analyze blood samples in the morning (8 pm), early afternoon (2 pm) and in the evening (7 pm) because diurnal patterns in neutrophil number and phenotype are prominent at these times of day in humans [14]. In particular, human neutrophils display a fresh-like phenotype (similar to murine ZT13) in the early morning and progress towards an aged-like phenotype (similar to murine ZT5) over the next 4-8 hours [14]. In our cohort we found that neutrophil counts increased over time and peaked at 2-7

pm (**Figure 6b**), while the granular-like phenotype of neutrophils decreased over time as hinted by changes in the side scattering properties by flow cytometry (**Figure 6c**). We confirmed the reduction in granule content by 3D reconstruction of human neutrophils stained for MPO, showing a trough at 2 pm (**Figure 6d-e**), as well as by TEM imaging (**Figure 6f**).

To assess whether these changes reflected proteomic changes as seen in murine neutrophils, we performed proteomic analyses of neutrophils extracted at 8 am and 2 pm from 5 different volunteers (**Supplementary Table 6**). Of the proteins detected, around 9.7% were differentially enriched at one or the other time of day ($p < 0.05$; **Supplementary Fig.9a**). Despite the relative low number, gene ontology analyses revealed changes in pathways related to vesicle-mediated transport, secretion, exocytosis or degranulation (**Supplementary Fig.9b** and **Supplementary Table 7**), which were consistent with the loss of granule content in human neutrophils over time. Although many of the individual proteins identified in the mouse analyses were not detected or did not show diurnal changes in the human samples (not shown), a finding that likely reflects the high variability among human individuals relative to co-housed and strain-matched mice, we were able to find numerous granule proteins in human neutrophils that were more abundant at 8am that at 2 pm (**Figure 6g**). Consistent with the findings in murine neutrophils, we found poor correlation between transcript and protein levels in human neutrophils (**Supplementary Fig.9d**), suggesting that the proteomic changes in human neutrophils are largely independent of transcriptional regulation. To assess whether loss of granule proteins also correlated with reduced NET-forming activity, we performed *ex vivo* assays of isolated neutrophils treated with vehicle or PMA. We found marked reductions in NET forming capacity over time (**Figure 6h-i**), following a temporal pattern that tightly matched the loss of granules (**Figure 6d**) and the elevated presence of NET-related proteins in the 8am group (**Supplementary Fig.9c**). These findings suggested that degranulation of neutrophils also takes place in the human circulation.

We finally questioned whether changes in proteome, granule content and NET-forming activity of human neutrophils might be associated with variations in the susceptibility to develop, and severity of, inflammation. In particular we focused on an existing cohort of community-acquired pneumonia (CAP) patients, which are at risk of developing acute respiratory distress syndrome (ARDS; [38]) and mechanistically mirrored our murine model in which low doses of endotoxin predispose to ALI [17, 28]. In a retrospective analysis of the human cohort we found that, among 5334 patients hospitalized with CAP, 125 (2.3%) developed ARDS, and we assessed the temporal patterns of disease onset and severity (using the pneumonia severity index) by plotting times of admission against the pneumonia scored index and death in this subset of patients.

Remarkably, we found consistent diurnal oscillations that were similar for both parameters, peaked in the morning (around 9 am) and progressively declined to reach a trough in the late afternoon (5-7 pm) (**Figure 6j**), a time that coincided with reduced granule content and low NET-forming activity in neutrophils (see **Figures 6d** and **6h**). Overall, these findings in healthy volunteers and in patients support the notion that proteomic disarming also occurs in human neutrophils, and may influence the incidence and severity of inflammation.

Discussion

The success of immunity in containing infections relies on a front-line of defensive cells bearing a pre-formed armamentarium of enzymes, anti-microbial peptides and specific receptors within internal granules, ready for rapid deployment upon encounter of pathogens or other danger signals. In the case of neutrophils, other strategies involving the release of NETs are now well-recognized [22] that, notably, require of granule-borne enzymes for proper chromatin disintegration [23]. Both discharge of granule content and NET-formation can be equally toxic for host cells and are in fact recurrent causes of co-lateral damage during sterile inflammation [39, 40]. Here, we demonstrate the existence of a cell-intrinsic program in neutrophils that, by inducing the progressive loss of granule proteins involved in inflammation and NET-formation, provide a previously unrecognized layer of protection against the toxic activity of these leukocytes. The proteome change occurs in the circulation, relies on components of a recently identified neutrophil timer and signaling through the chemokine receptor CXCR2 and its ligand CXCL2 [14] (summarized in **Supplementary Fig.10** and **MovieS6**). We note that the phenomenon of proteome disarming described herein shares key features with a process of neutrophil “aging” reported recently[14]; both rely on CXCL2/CXCR2 signaling, are regulated by Bmal1 and CXCR4 in a cell-intrinsic manner, and display similar temporal patterns (i.e., peak at noon). This suggests that both processes may represent distinct manifestations of a core circadian program in neutrophils that allows anticipation of potential threats[14], while at the same time protects the hosts from excessive inflammation, vascular damage, and death.

Beyond regulating the magnitude of inflammation, an important finding is that changes in the neutrophil proteome display temporal oscillations that align neutrophil activity with circadian cycles. This observation is of particular interest given the important regulatory roles of the mammalian circadian clock in various aspects of innate immunity [41]. For example, a Bmal1-driven intrinsic clock regulates the migration of Ly6C^{hi} inflammatory monocytes between the

circulation and tissues, and temporally gates the production of inflammatory cytokines thus reducing the vulnerability to septic shock [42], and transcriptional regulation of *Tlr9* in macrophages dictates the long-term response to antigens depending on the time of vaccination [43]. Similar transcriptional regulation dictates changes in the migration of neutrophils, and allows infiltration of naïve tissues in anticipation of potential infections [14]. Different from these transcription-mediated regulatory mechanisms, however, we uncover a different type of circadian regulation of the neutrophil proteome that blunts their capacity to release toxic mediators and to produce NETs. This level of immune regulation may be particularly relevant for granulocytes, a group of innate immune cells that synthesize and store the majority of their early-response mediators (i.e., proteases, antimicrobial peptides and respiratory burst oxidase) inside dedicated organelles. Because the formation of granules and their content occurs as neutrophils differentiate inside bone marrow [7, 44], it is unlikely that the changes in the granule proteome shown here in the circulation are transcriptionally regulated, as illustrated by the poor correlation found between the proteome and the transcriptome of these cells. These findings provide one of the few examples of circadian regulatory programs not driven by direct transcriptional regulation, perhaps reminiscent of redox regulation in red blood cells in which the lack of nucleus precludes canonical regulation of their proteome [45]. Unique to neutrophils, however, the data suggests a model in which upstream control of *Cxcl2* transcription by Bmal1 [14] allows indirect regulation of the neutrophil's proteome by the canonical circadian machinery. Conceptually, the temporal nature of this process in blood aligns with the evolutionary value of circadian oscillations in segregating mutually antagonistic processes, in this case potent anti-microbial responses and protection of the host's own cells.

The circadian patterns in granule content and elastase activity in plasma suggested progressive discharge of granules while in the circulation, such that neutrophils that migrate into tissues during the day [11] may have lost part of their anti-microbial arsenal but are at the same time less likely to elicit organ damage as shown in the ALI model. Because neutrophil proteases are additionally important to activate many biological mediators, including cytokines, chemokines, growth factors as well as adhesion and pattern-recognition receptors [46, 47], and even modulate signaling cascades in other cells [48, 49], the programmed proteome change reported here may have pleiotropic consequences in physiology. For instance, it predicts that neutrophils that are newly released from the bone marrow in conditions of stress, such as obesity or cancer [50, 51], may be better suited to regulate physiological aspects of target organs than aged neutrophils that enter organs at the end of their life cycle and have lost part of their cargo.

The studies in the ALI model and the temporal patterns of granule content also shed light into the particular susceptibility of lungs to diurnal inflammation. Indeed, previous studies have shown that large numbers of neutrophils marginate within the pulmonary microcirculation in mice, rabbits and non-human primates after stimulation or in the steady-state [11, 20, 52], and suggested that the lungs can provide a niche for effective anti-microbial responses [53]. The homeostatic accumulation of neutrophils in this organ at the end of the light cycle in mice [11] would predict higher susceptibility to inflammatory stimuli at this time. However, we find that neutrophils recovered from naïve lungs have reduced granularity, and that mutants with constitutive low levels of granules in neutrophils display permanent protection from ALI, together highlighting a dominant contribution of the mechanism described herein for tissue protection. Nonetheless, we predict that these protective mechanisms intrinsic to neutrophils cooperate with others imprinted in parenchymal lung cells that are similarly subjected to robust circadian regulation [54].

It has long been recognized that multiple inflammatory processes in humans display circadian periodicity [55], and experimental models and retrospective studies have corroborated that not only the onset of inflammation, but also the severity of the inflammatory events manifests diurnal oscillations [37]. These events are often caused by neutrophil activation and by thrombosis, which in turn can be exacerbated in the presence of neutrophils or NETs [17, 30, 56, 57]. Thus, our current findings in the context of ALI may extend to other inflammatory and thrombotic conditions affecting multiple organs, and suggests that interventions aimed at inducing controlled degranulation may effectively "disarm" neutrophils and protect organs from catastrophic inflammation.

Supplementary Information

The Supplementary Information file contains Supplementary Figures 1-10 and legends for Movies S1-6 and Supplementary Tables 1-8.

Acknowledgments

We thank members of the Comparative Medicine Unit and Advanced microscopy Unit at CNIC. This study was supported by Intramural grants from the Severo Ochoa program (IGP-SO), grant from Fundació La Marató de TV3 (120/C/2015-20153032), and grant SAF2015-65607-R from Ministerio de Ciencia, Investigacion y Universidades (MCIU), and co-funding by Fondo Europeo de Desarrollo Regional (FEDER) to A.H. Fellowship BES-2013-065550 from MCIU to J.M.A, and

fellowship Health-PERIS 2016–2020 to C.C. Funds were also obtained from Instituto de Salud Carlos III (ISCIII) FIS PI17/01601 to I.L. and SAF2015-68632-R from MCIU to M.A.M.; Welcome Trust Seed Award in Science (206103/Z/17/Z) to D.R., SFB1123-A1/A10 from Deutsche Forschungsgemeinschaft and ERC-AdG 692511 to C.W. ; SAF2017-84494-C2-R and Programa Red Guipuzcoana de Ciencia, Tecnología e Información 2018-CIEN-000058-01 to J.R-C. Work at CIC biomaGUNE was performed under the Maria de Maeztu Units of Excellence Program from the Spanish State Research Agency (MDM-2017-0720). The CNIC is supported by the MCIU and the Pro-CNIC Foundation, and is a Severo Ochoa Center of Excellence (MEIC award SEV-2015-0505).

Author contribution: J.M.A, A.A.C, G.C., E.B.K., E.C., and Y.R.V. performed experiments. J.M.A., D.R. and A.R.P. performed bioinformatic analysis. F.O. obtained human samples. C.W., M.A.M., J.R-C., I.L. and J.V. contributed essential reagents, equipment, expertise and funds. C.C. and A.T. contributed clinical data. J.M.A. and A.H. designed and supervised experiments, and wrote the manuscript, which was edited by all authors.

Author Information: Reprints and permissions information are available at www.nature.com/reprints. The authors declare no competing financial interests. Correspondence and requests for materials should be addressed to ahidalgo@cnic.es

References

1. Cowland JB, Borregaard N. Granulopoiesis and granules of human neutrophils. *Immunol Rev* 2016, **273**(1)**:** 11-28.

2. Ley K, Hoffman HM, Kubes P, Cassatella MA, Zychlinsky A, Hedrick CC*, et al.* Neutrophils: New insights and open questions. *Sci Immunol* 2018, **3**(30).

3. Borregaard N, Sorensen OE, Theilgaard-Monch K. Neutrophil granules: a library of innate immunity proteins. *Trends Immunol* 2007, **28**(8)**:** 340-345.

4. Rorvig S, Ostergaard O, Heegaard NH, Borregaard N. Proteome profiling of human neutrophil granule subsets, secretory vesicles, and cell membrane: correlation with transcriptome profiling of neutrophil precursors. *J Leukoc Biol* 2013, **94**(4)**:** 711-721.

5. Borregaard N. Neutrophils, from marrow to microbes. *Immunity* 2010, **33**(5)**:** 657-670.

6. Le Cabec V, Cowland JB, Calafat J, Borregaard N. Targeting of proteins to granule subsets is determined by timing and not by sorting: The specific granule protein NGAL is localized to azurophil granules when expressed in HL-60 cells. *Proc Natl Acad Sci U S A* 1996, **93**(13)**:** 6454-6457.

7. Evrard M, Kwok IWH, Chong SZ, Teng KWW, Becht E, Chen J*, et al.* Developmental Analysis of Bone Marrow Neutrophils Reveals Populations Specialized in Expansion, Trafficking, and Effector Functions. *Immunity* 2018, **48**(2)**:** 364-379 e368.

8. Grassi L, Pourfarzad F, Ullrich S, Merkel A, Were F, Carrillo-de-Santa-Pau E*, et al.* Dynamics of Transcription Regulation in Human Bone Marrow Myeloid Differentiation to Mature Blood Neutrophils. *Cell Rep* 2018, **24**(10)**:** 2784-2794.

9. Pillay J, den Braber I, Vrisekoop N, Kwast LM, de Boer RJ, Borghans JA*, et al.* In vivo labeling with 2H2O reveals a human neutrophil lifespan of 5.4 days. *Blood* 2010, **116**(4)**:** 625-627.

10. Tak T, Tesselaar K, Pillay J, Borghans JA, Koenderman L. What's your age again? Determination of human neutrophil half-lives revisited. *J Leukoc Biol* 2013, **94**(4)**:** 595-601.

11. Casanova-Acebes M, Nicolas-Avila JA, Li JL, Garcia-Silva S, Balachander A, Rubio-Ponce A*, et al.* Neutrophils instruct homeostatic and pathological states in naive tissues. *J Exp Med* 2018, **215**(11)**:** 2778-2795.

12. He W, Holtkamp S, Hergenhan SM, Kraus K, de Juan A, Weber J*, et al.* Circadian Expression of Migratory Factors Establishes Lineage-Specific Signatures that Guide the Homing of Leukocyte Subsets to Tissues. *Immunity* 2018, **49**(6)**:** 1175-1190 e1177.

13. Adrover JM, Nicolas-Avila JA, Hidalgo A. Aging: A Temporal Dimension for Neutrophils. *Trends Immunol* 2016, **37**(5)**:** 334-345.

14. Adrover JM, Del Fresno C, Crainiciuc G, Cuartero MI, Casanova-Acebes M, Weiss LA*, et al.* A Neutrophil Timer Coordinates Immune Defense and Vascular Protection. *Immunity* 2019.

15. Grommes J, Soehnlein O. Contribution of neutrophils to acute lung injury. *Mol Med* 2011, **17**(3-4)**:** 293-307.

16. Looney MR, Su X, Van Ziffle JA, Lowell CA, Matthay MA. Neutrophils and their Fc gamma receptors are essential in a mouse model of transfusion-related acute lung injury. *The Journal of clinical investigation* 2006, **116**(6)**:** 1615-1623.

17. Sreeramkumar V, Adrover JM, Ballesteros I, Cuartero MI, Rossaint J, Bilbao I*, et al.* Neutrophils scan for activated platelets to initiate inflammation. *Science* 2014, **346**(6214)**:** 1234-1238.

18. Matthay MA, Zemans RL. The acute respiratory distress syndrome: pathogenesis and treatment. *Annual review of pathology* 2011, **6:** 147-163.

19. Casanova-Acebes M, Pitaval C, Weiss LA, Nombela-Arrieta C, Chevre R, N AG*, et al.* Rhythmic modulation of the hematopoietic niche through neutrophil clearance. *Cell* 2013, **153**(5)**:** 1025-1035.

20. Devi S, Wang Y, Chew WK, Lima R, N AG, Mattar CN*, et al.* Neutrophil mobilization via plerixafor-mediated CXCR4 inhibition arises from lung demargination and blockade of neutrophil homing to the bone marrow. *J Exp Med* 2013, **210**(11)**:** 2321-2336.

21. Zhang D, Chen G, Manwani D, Mortha A, Xu C, Faith JJ*, et al.* Neutrophil ageing is regulated by the microbiome. *Nature* 2015, **525**(7570)**:** 528-532.

22. Papayannopoulos V. Neutrophil extracellular traps in immunity and disease. *Nat Rev Immunol* 2018, **18**(2)**:** 134-147.

23. Papayannopoulos V, Metzler KD, Hakkim A, Zychlinsky A. Neutrophil elastase and myeloperoxidase regulate the formation of neutrophil extracellular traps. *J Cell Biol* 2010, **191**(3)**:** 677-691.

24. Urban CF, Ermert D, Schmid M, Abu-Abed U, Goosmann C, Nacken W*, et al.* Neutrophil extracellular traps contain calprotectin, a cytosolic protein complex involved in host defense against Candida albicans. *PLoS Pathog* 2009, **5**(10)**:** e1000639.

25. Csepregi JZ, Orosz A, Zajta E, Kasa O, Nemeth T, Simon E*, et al.* Myeloid-Specific Deletion of Mcl-1 Yields Severely Neutropenic Mice That Survive and Breed in Homozygous Form. *Journal of immunology* 2018, **201**(12)**:** 3793-3803.

26. Kolaczkowska E, Kubes P. Neutrophil recruitment and function in health and inflammation. *Nat Rev Immunol* 2013, **13**(3)**:** 159-175.

27. Phillipson M, Kubes P. The neutrophil in vascular inflammation. *Nat Med* 2011, **17**(11)**:** 1381-1390.

28. Looney MR, Nguyen JX, Hu Y, Van Ziffle JA, Lowell CA, Matthay MA. Platelet depletion and aspirin treatment protect mice in a two-event model of transfusion-related acute lung injury. *The Journal of clinical investigation* 2009, **119**(11)**:** 3450-3461.

29. Caudrillier A, Kessenbrock K, Gilliss BM, Nguyen JX, Marques MB, Monestier M*, et al.* Platelets induce neutrophil extracellular traps in transfusion-related acute lung injury. *The Journal of clinical investigation* 2012, **122**(7)**:** 2661-2671.

30. Hidalgo A, Chang J, Jang JE, Peired AJ, Chiang EY, Frenette PS. Heterotypic interactions enabled by polarized neutrophil microdomains mediate thromboinflammatory injury. *Nat Med* 2009, **15**(4)**:** 384-391.

31. Thomas GM, Carbo C, Curtis BR, Martinod K, Mazo IB, Schatzberg D*, et al.* Extracellular DNA traps are associated with the pathogenesis of TRALI in humans and mice. *Blood* 2012, **119**(26)**:** 6335-6343.

32. Looney MR, Gilliss BM, Matthay MA. Pathophysiology of transfusion-related acute lung injury. *Current opinion in hematology* 2010, **17**(5)**:** 418-423.

33. Looney MR, Thornton EE, Sen D, Lamm WJ, Glenny RW, Krummel MF. Stabilized imaging of immune surveillance in the mouse lung. *Nature methods* 2011, **8**(1)**:** 91-96.

34. Strieter RM, Keane MP, Burdick MD, Sakkour A, Murray LA, Belperio JA. The role of CXCR2/CXCR2 ligands in acute lung injury. *Curr Drug Targets Inflamm Allergy* 2005, **4**(3)**:** 299-303.

35. Muller JE, Stone PH, Turi ZG, Rutherford JD, Czeisler CA, Parker C*, et al.* Circadian variation in the frequency of onset of acute myocardial infarction. *The New England journal of medicine* 1985, **313**(21)**:** 1315-1322.

36. Scheiermann C, Kunisaki Y, Frenette PS. Circadian control of the immune system. *Nat Rev Immunol* 2013, **13**(3)**:** 190-198.

37. Suarez-Barrientos A, Lopez-Romero P, Vivas D, Castro-Ferreira F, Nunez-Gil I, Franco E*, et al.* Circadian variations of infarct size in acute myocardial infarction. *Heart* 2011, **97**(12)**:** 970-976.

38. Cilloniz C, Ferrer M, Liapikou A, Garcia-Vidal C, Gabarrus A, Ceccato A*, et al.* Acute respiratory distress syndrome in mechanically ventilated patients with community-acquired pneumonia. *Eur Respir J* 2018, **51**(3).

39. Castanheira F, Kubes P. Neutrophils and NETS in modulating acute and chronic inflammation. *Blood* 2019.

40. Gomez-Moreno D, Adrover JM, Hidalgo A. Neutrophils as effectors of vascular inflammation. *Eur J Clin Invest* 2018, **48 Suppl 2:** e12940.

41. Man K, Loudon A, Chawla A. Immunity around the clock. *Science* 2016, **354**(6315)**:** 999-1003.

42. Nguyen KD, Fentress SJ, Qiu Y, Yun K, Cox JS, Chawla A. Circadian gene Bmal1 regulates diurnal oscillations of Ly6C(hi) inflammatory monocytes. *Science* 2013, **341**(6153)**:** 1483-1488.

43. Silver AC, Arjona A, Walker WE, Fikrig E. The circadian clock controls toll-like receptor 9-mediated innate and adaptive immunity. *Immunity* 2012, **36**(2)**:** 251-261.

44. Faurschou M, Borregaard N. Neutrophil granules and secretory vesicles in inflammation. *Microbes Infect* 2003, **5**(14)**:** 1317-1327.

45. O'Neill JS, Reddy AB. Circadian clocks in human red blood cells. *Nature* 2011, **469**(7331)**:** 498-503.

46. Meyer-Hoffert U. Neutrophil-derived serine proteases modulate innate immune responses. *Front Biosci (Landmark Ed)* 2009, **14:** 3409-3418.

47. Pham CT. Neutrophil serine proteases: specific regulators of inflammation. *Nat Rev Immunol* 2006, **6**(7)**:** 541-550.

48. Houghton AM, Rzymkiewicz DM, Ji H, Gregory AD, Egea EE, Metz HE*, et al.* Neutrophil elastase-mediated degradation of IRS-1 accelerates lung tumor growth. *Nat Med* 2010, **16**(2)**:** 219-223.

49. Talukdar S, Oh DY, Bandyopadhyay G, Li D, Xu J, McNelis J*, et al.* Neutrophils mediate insulin resistance in mice fed a high-fat diet through secreted elastase. *Nat Med* 2012, **18**(9)**:** 1407-1412.

50. Coffelt SB, Kersten K, Doornebal CW, Weiden J, Vrijland K, Hau CS*, et al.* IL-17-producing gammadelta T cells and neutrophils conspire to promote breast cancer metastasis. *Nature* 2015, **522**(7556)**:** 345-348.

51. Quail DF, Olson OC, Bhardwaj P, Walsh LA, Akkari L, Quick ML*, et al.* Obesity alters the lung myeloid cell landscape to enhance breast cancer metastasis through IL5 and GM-CSF. *Nat Cell Biol* 2017, **19**(8)**:** 974-987.

52. Doerschuk CM. The role of CD18-mediated adhesion in neutrophil sequestration induced by infusion of activated plasma in rabbits. *American journal of respiratory cell and molecular biology* 1992, **7**(2)**:** 140-148.

53. Yipp BG, Kim JH, Lima R, Zbytnuik LD, Petri B, Swanlund N*, et al.* The Lung is a Host Defense Niche for Immediate Neutrophil-Mediated Vascular Protection. *Sci Immunol* 2017, **2**(10).

54. Gibbs J, Ince L, Matthews L, Mei J, Bell T, Yang N*, et al.* An epithelial circadian clock controls pulmonary inflammation and glucocorticoid action. *Nat Med* 2014, **20**(8)**:** 919-926.

55. Muller JE, Tofler GH. Circadian variation and cardiovascular disease. *The New England journal of medicine* 1991, **325**(14)**:** 1038-1039.

56. Engelmann B, Massberg S. Thrombosis as an intravascular effector of innate immunity. *Nat Rev Immunol* 2013, **13**(1)**:** 34-45.

57. Jimenez-Alcazar M, Rangaswamy C, Panda R, Bitterling J, Simsek YJ, Long AT*, et al.* Host DNases prevent vascular occlusion by neutrophil extracellular traps. *Science* 2017, **358**(6367)**:** 1202-1206.

58. Navarro P, Trevisan-Herraz M, Bonzon-Kulichenko E, Nunez E, Martinez-Acedo P, Perez-Hernandez D*, et al.* General statistical framework for quantitative proteomics by stable isotope labeling. *J Proteome Res* 2014, **13**(3)**:** 1234-1247.

59. Garcia-Marques F, Trevisan-Herraz M, Martinez-Martinez S, Camafeita E, Jorge I, Lopez JA*, et al.* A Novel Systems-Biology Algorithm for the Analysis of Coordinated Protein Responses Using Quantitative Proteomics. *Mol Cell Proteomics* 2016, **15**(5)**:** 1740-1760.

60. Trevisan-Herraz M, Bagwan N, Garcia-Marques F, Rodriguez JM, Jorge I, Ezkurdia I*, et al.* SanXoT: a modular and versatile package for the quantitative analysis of high-throughput proteomics experiments. *Bioinformatics* 2019, **35**(9)**:** 1594-1596.

Figures and Figure legends

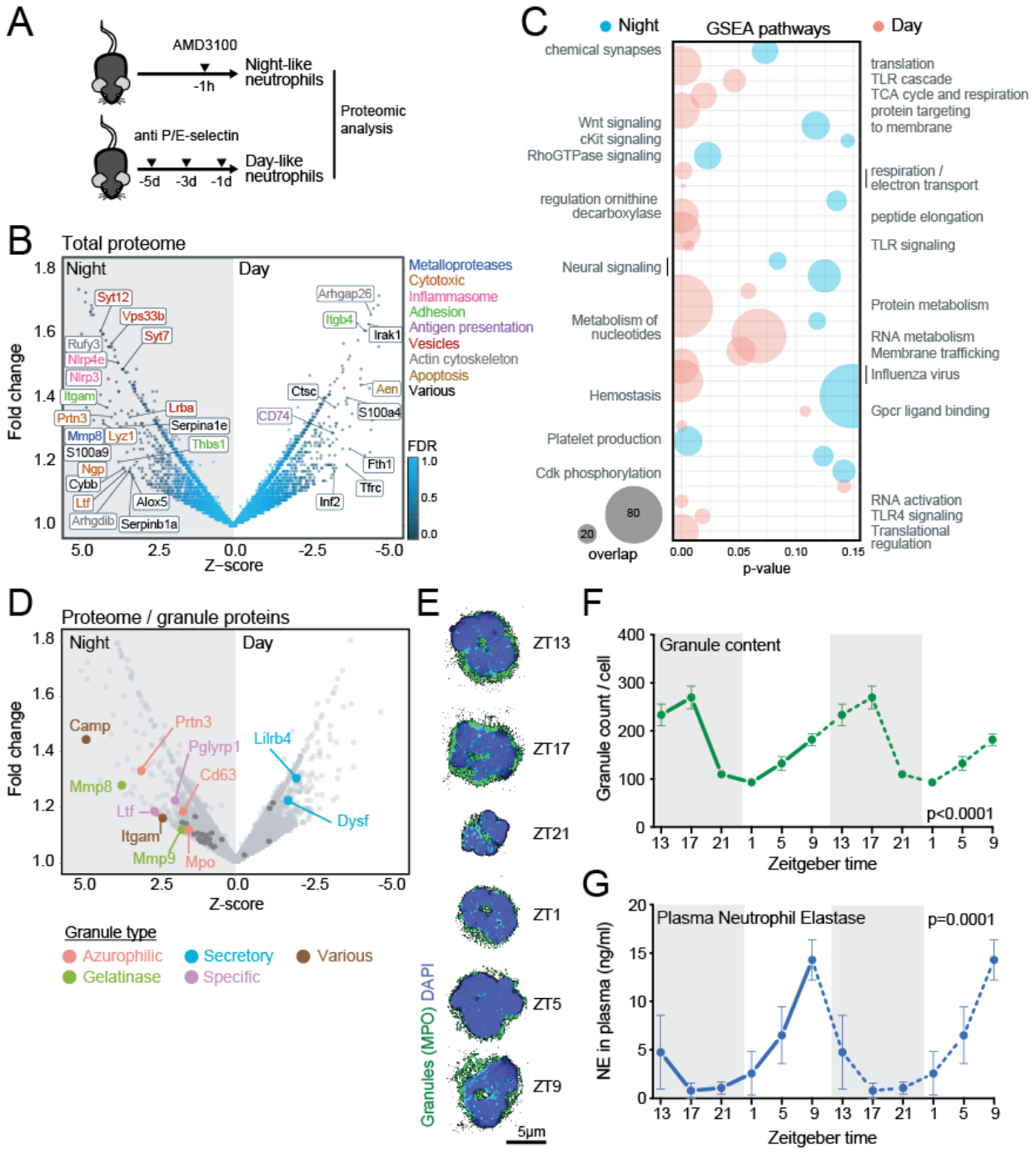

Figure 1. Diurnal changes in the neutrophil proteome.
(A) Experimental strategy for proteomic analysis of aged and fresh neutrophils. (B) Volcano plot of proteins with a False Discovery Rate (FDR) < 0.01. A positive Z-score represents an increase in nighttime (fresh) over daytime (aged) neutrophils. Color represents the functional category for each protein (legend, top-right). (C) Gene-set enrichment analysis of the proteomics data showing

pathways with a p-value < 0.15 enriched in aged (red) or fresh (blue) neutrophils. Size of the bubble-plot represents overlap between query and gene-set (legend bottom-right). (D) Volcano plot of the proteomic dataset showing granule proteins with a Z-score > 2. Colors show the granule type for each protein. (E) Z-stack maximum projection of neutrophils stained for primary granules with MPO and counterstained with DAPI. (F) Quantification of neutrophil granule contents during a full diurnal cycle. Curves are repeated (dashed line) to better appreciate the circadian pattern. Dark phase is shown in grey; n=30 cells per time point. G) Neutrophil elastase activity in plasma. Curves are repeated (dashed line) to better appreciate the circadian pattern. Dark phase is shown in grey; n=4 mice per time point. Data in (F, G) are shown as mean ± SEM, and p-values were determined by amplitude vs. zero t-test analysis (see Methods).

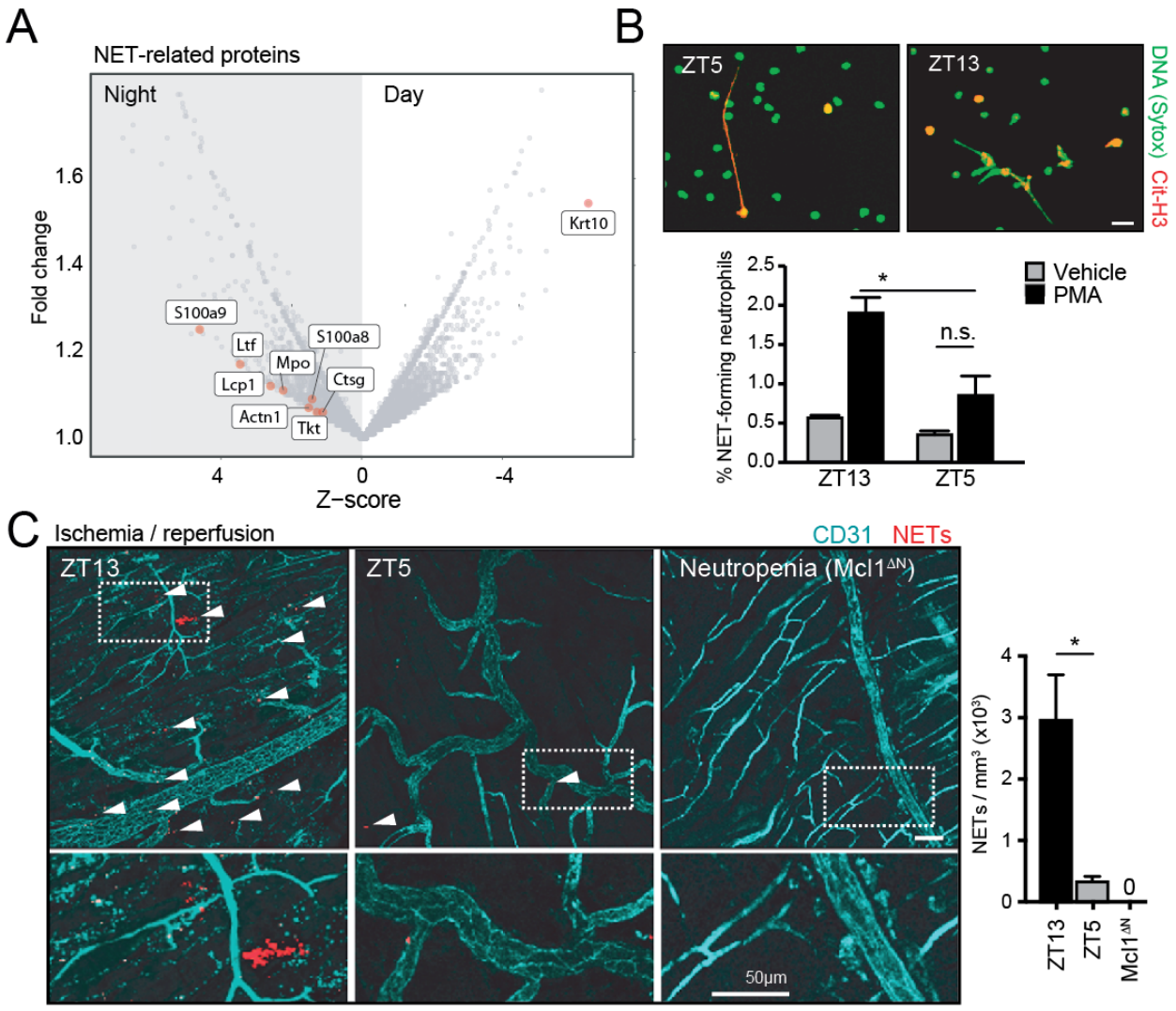

Figure 2. Diurnal loss of NET-forming capacity.

(A) Volcano plot of the neutrophil proteome showing proteins found in NETs (red dots), and enrichment of these proteins in nighttime neutrophils. (B) *Ex vivo* NET-formation assay. Neutrophils sorted at ZT13 (nighttime) or ZT5 (daytime) were stimulated with PMA or vehicle to induce NETs and stained for citrunillated-histone 3 (Cit-H3) and DNA (top). Colocalization of both markers was used to quantify NET formation as shown in the bar graph (bottom); n=3 mice per time point. (C) Representative images (left) and quantification (right) of in vivo NET formation in the cremaster muscle subjected to ischemia/reperfusion at nighttime (ZT13), or at daytime (ZT5). Triple colocalization of MPO, DNA and Cit-H3 was used to define and quantify the area of NETs (red; arrowheads). Neutropenic Mcl1$^{\Delta N}$ mice (Lyz2^{Cre}; Mcl1$^{fl/fl}$ mice) were used as controls and showed no NETs. Dotted areas are showed magnified in bottom panels; n = 3 mice per condition. Scale bars, 50 µm. Bars show mean ± SEM. *; p<0.05; n.s., not significant, as determined by unpaired t-test analysis.

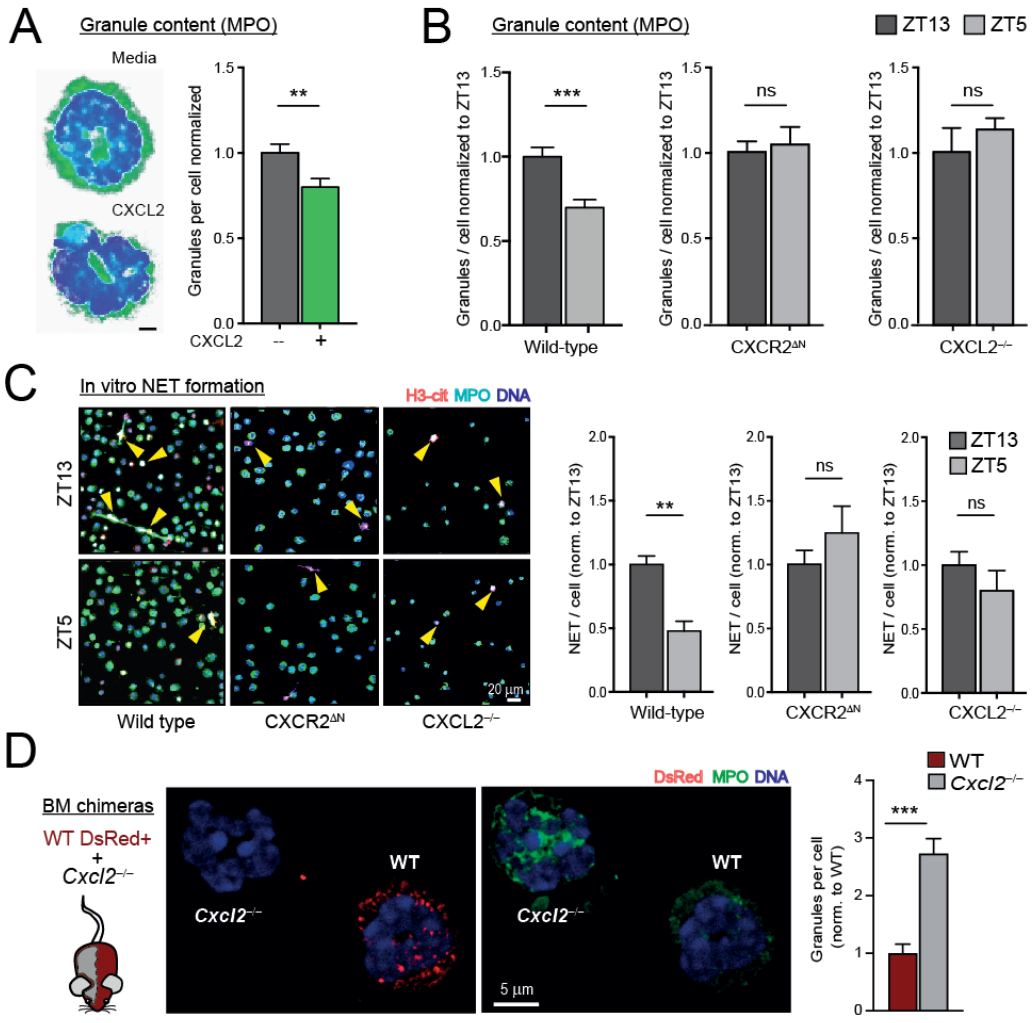

Figure 3. Degranulation and loss of NET-forming capacity are driven by CXCL2/CXCR2 signaling.

(A) Ex-vivo stimulation of sorted neutrophils with CXCL2 induces degranulation (right), as quantified by confocal imaging of MPO-stained neutrophils (left); n = 29-32 cells. (B) Diurnal quantification of granule content in neutrophils from WT, CXCR2$^{\Delta N}$ or CXCL2$^{-/-}$ mice, showing a loss of diurnal fluctuation in CXCR2-defici

ent (n = 38-40 cells) or CXCL2-deficient neutrophils (n = 15-31), compared to their WT counterparts (n = 30-33 cells per time point). (C) Ex-vivo NET formation assays with sorted neutrophils stimulated with PMA or vehicle control, at nighttime (ZT13) or daytime (ZT5). NETs were quantified by triple-colocalization of citrunillated-histone 3, DNA and MPO in confocal micrographs (left). Each mouse was normalized to its vehicle control and NET formation at ZT13 and ZT5 compared (right). CXCL2-deficient (n = 3 mice per time) and CXCR2-deficient (n = 2-6 mice per time) neutrophils showed loss of diurnal fluctuation in NET formation compared with WT cells (n = 4-6 mice per time). (D) CXCL2 signaling causes degranulation cell-autonomously, as shown by analysis of MPO+ granules in neutrophils from BM chimeras reconstituted with DsRed+ wild-type and DsRed^{NEG} *Cxcl2*$^{-/-}$ donors; n = 3 mice. Bars show mean ± SEM. **; p<0.01; n.s., not significant, as determined by paired (A) or unpaired (B-C) t-test analysis.

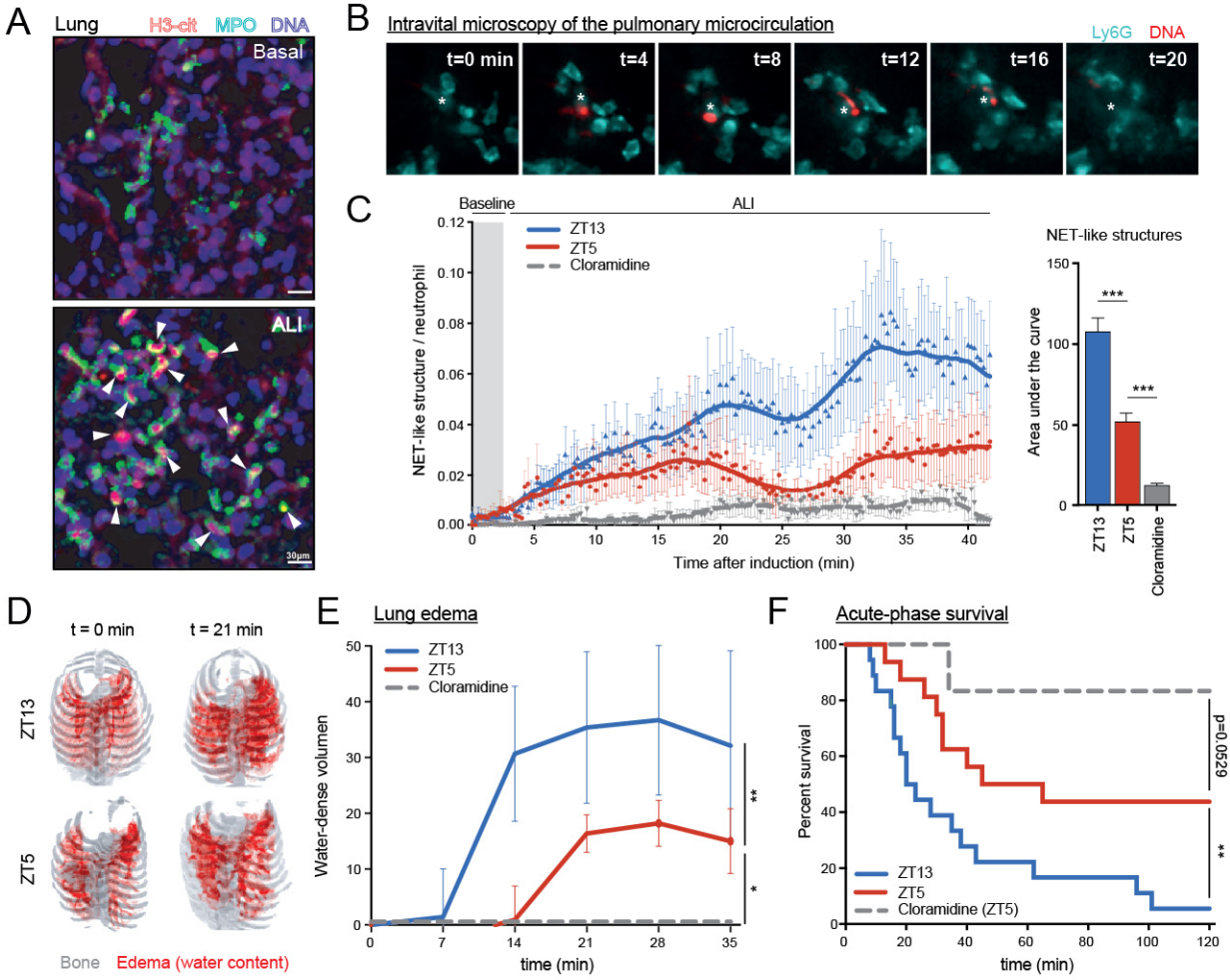

Figure 4. Diurnal loss of NET formation and pulmonary protection during ALI.
(A) Presence of NETs in lungs. Shown are maximum projections of confocal Z-stack series of cleared lungs from control mice (Basal) or mice with antibody-induced acute lung injury induction (ALI). Lungs were stained against citrunillated-histone 3, MPO and DNA, and some NETs are shown (arrowheads). (B) Time-series of 4D intravital imaging captures of NET-like structures in the lungs of ALI-induced mice. NET-like structures were defined as free DNA extruded out of Ly6G+ neutrophils. See also **Movie S1.** (C) Quantification of NET-like structures as shown in (B), and normalized to the number of neutrophils in mice in which ALI was performed at nighttime (ZT13) or daytime (ZT5), or in mice treated with Cl-amidine (at ZT5). Time course (left panel) and area under the curve values (right panel); n = 15 fields from 4 mice per condition. (D) Representative images of longitudinal CT series of edema formation at 0 or 21 min after inducing ALI ZT13 or ZT5. Note the increased edema (red) at night. Background bone signal (grey) is shown for anatomical positioning. (E) Quantification of the images in (D). Volume of edema was increased at ZT13 (blue; n = 7) relative to ZT5 (red; n = 7). Mice treated with Cl-amidine are shown as a control (grey, n = 4). (F) Survival of mice subjected to ALI at ZT13 (blue) or ZT5 (red), or treated with Cl-amidine (gray); n = 11-21 mice. Data are shown as mean ± SEM. **; p<0.01; ***, p<0.001, as determined by one-way ANOVA with Dunnet's multiple comparison test (C), two-way ANOVA (E) or log rank (Mantel-Cox) test (F).

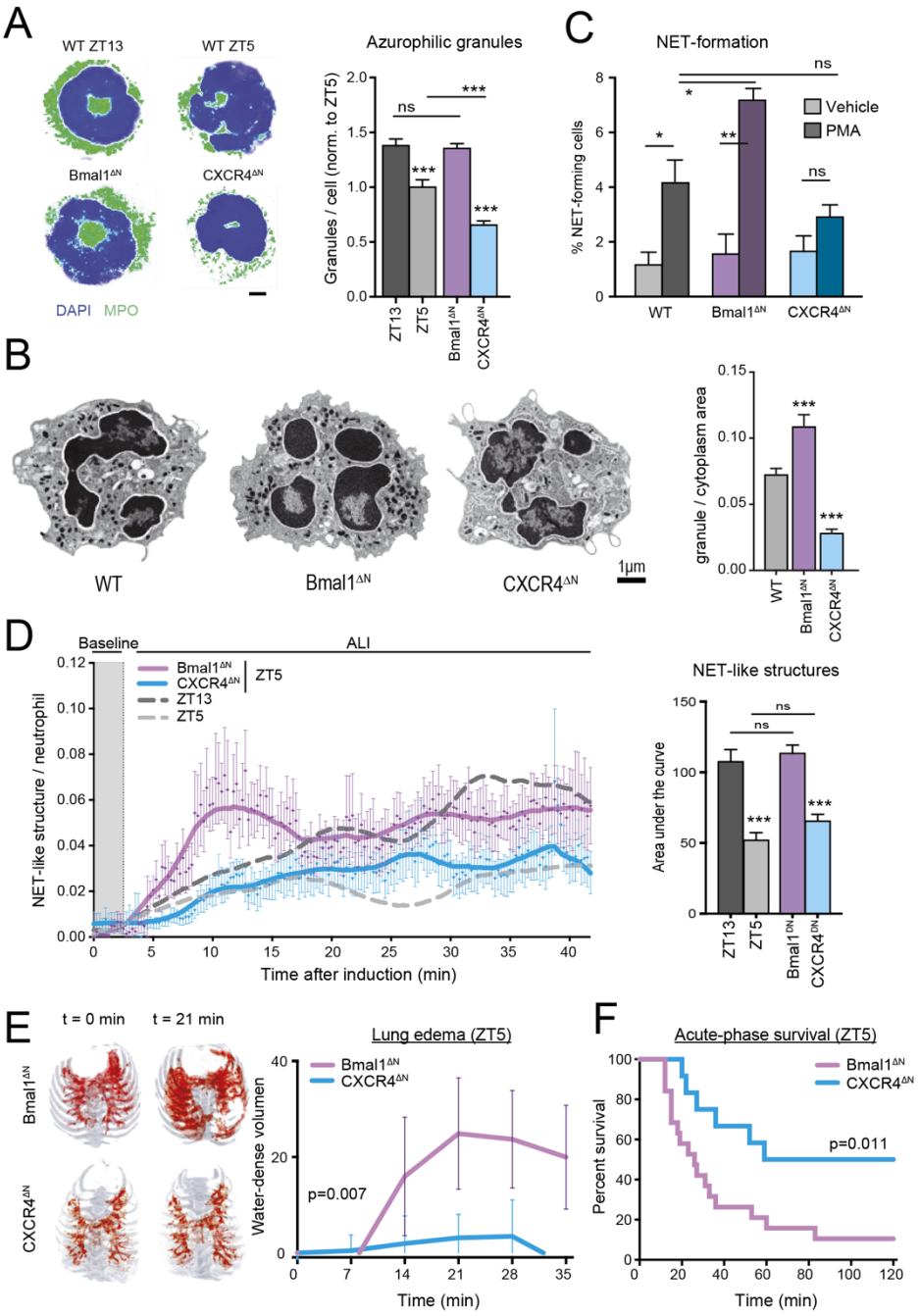

Figure 5. Diurnal degranulation and pulmonary protection is neutrophil-intrinsic.
(A) Confocal micrographs and quantification of primary granules in neutrophils from WT mice at night (ZT13) or daytime (ZT5), and from mutant mice (both at ZT5); n = 30-50 cells from 3 mice. (B) Transmission electron microscopy images (left), and quantification of electrodense azurophilic granules (right) in WT and mutant mice (all at ZT5), showing increased granule content in Bmal1$^{\Delta N}$, and reduced in CXCR4$^{\Delta N}$ neutrophils compared with WT cells; n = 19. (C) *Ex vivo* NET formation in sorted WT, Bmal1$^{\Delta N}$ or CXCR4$^{\Delta N}$ neutrophils stimulated with PMA or vehicle as control; n = 3 per condition. (D) Quantification of NET-like structures normalized to the number of

neutrophils during ALI in Bmal1$^{\Delta N}$ or CXCR4$^{\Delta N}$ mice. Time course and elevations from baseline (gray area) are shown in the left panel, and the areas under the curve are shown in the right panel. Experiments were performed at ZT5. Data from wild-type mice at ZT5 and ZT13 (from **Figure 4C**) are shown for reference; n = 15 fields from 3 mice per condition. (E) Representative images of longitudinal CT series of edema (red) in mutant mice subject to ALI (left), and quantification of the edema volume over time (right panel); n = 7 mice per genotype. (F) Survival curves of Bmal1$^{\Delta N}$ and CXCR4$^{\Delta N}$ mice subjected to ALI; n = 12-19 mice per genotype. Data are shown as mean ± SEM. *; $p<0.05$; **, $p<0.01$; ***, $p<0.001$; n.s., not significant, as determined by one-way ANOVA with Dunnet's multiple comparison test (A-D), two-way ANOVA (E) or log rank (Mantel-Cox) test (F).

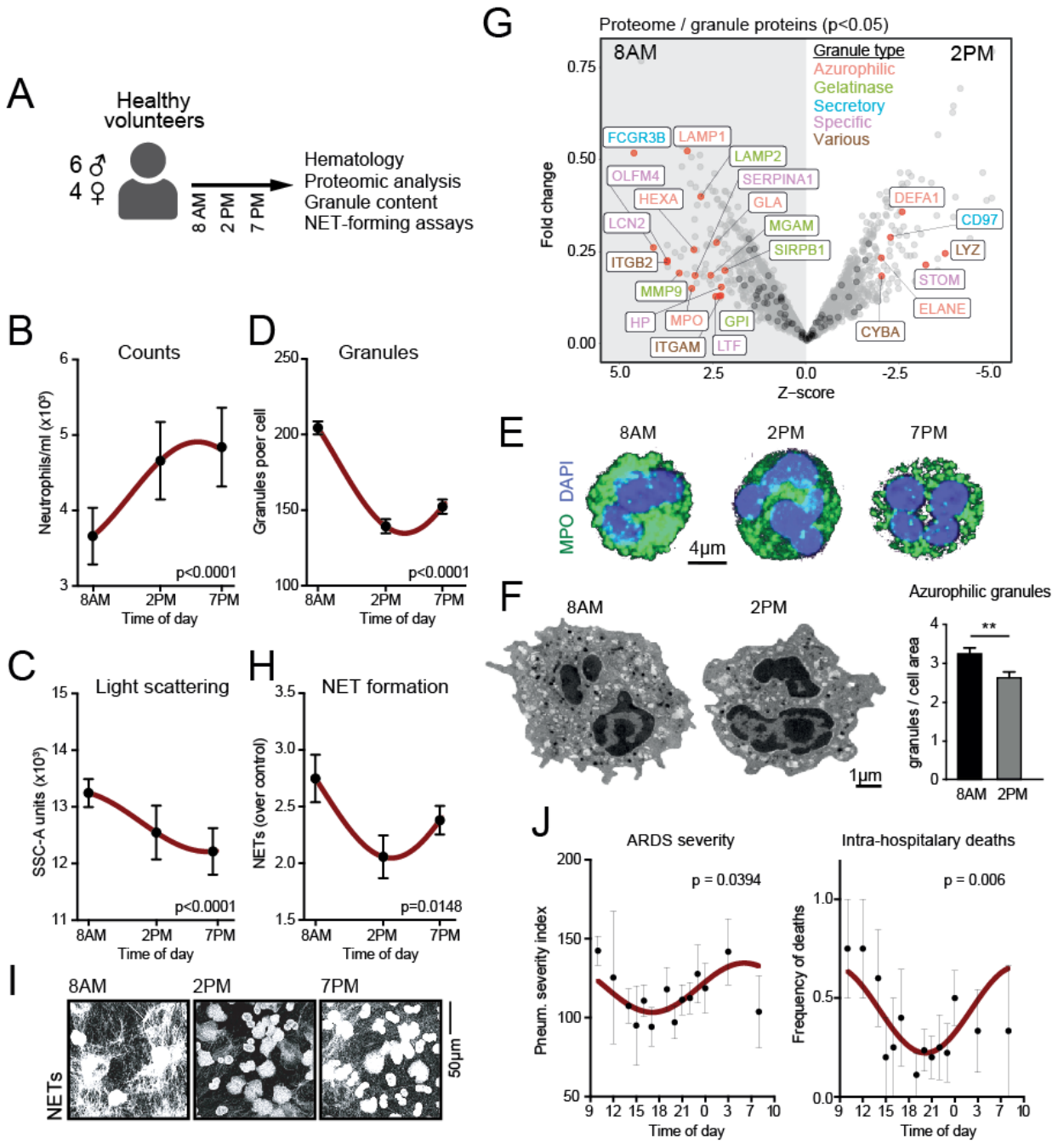

Figure 6. Evidence for neutrophil disarming and pulmonary protection in humans.
(A) Experimental design. Blood from 10 healthy volunteers was extracted at 8 am, 2pm and 7 pm. Neutrophils were purified for proteomic analysis, granule quantification and NET-formation assays. (B) Blood neutrophil counts in human volunteers at the different time points; n = 10. (C) Light scattering (SSC-A) values for human neutrophils at different times, as measured by flow cytometry; n = 10 human volunteers. (D) Quantification of primary granules from confocal images of human neutrophils from images in (E); n = 150 cells from 10 volunteers. (E) Representative images of granule content of human neutrophils. (F) Transmission electron micrographs (left) of

human neutrophils in the morning (8 am) and early afternoon (2 pm) showing reduced numbers of electrodense primary granules (right); n = 33 cells from 3 human volunteers. (G) Volcano plot of granule proteins in the human neutrophil proteome, showing higher content in granule proteins (color-coded) at 8 am compared with 2 pm; n = 5 samples from healthy volunteers. Red dots and labels show differentially expressed proteins with p-value<0.05, and black dots show all granule proteins. Label color indicates the granule type in which the protein is normally found (bottom right). (H) Quantification of *ex vivo* NET formation by human neutrophils stimulated with PMA or vehicle at the indicated time points. Representative confocal images of the PMA-induced NETs are shown in (I); n = 10 volunteers. (J) Acute respiratory distress syndrome (ARDS) severity shown as the pneumonia severity index (left) and intra-hospitalary deaths (right), of patients entering the ICU at different times of the day; n = 125 patients. Data are shown as mean ± SEM. **; p<0.01, as determined by unpaired t-test analysis (F). P values for the circadian plots were calculated by the amplitude vs. zero t-test analysis (B-D, H, J).

Methods

Mice

All experiments were performed in 7 to 18 week-old male C57BL/6 or Balb/c mice kept in a specific pathogen-free facility at Centro Nacional de Investigaciones Cardiovasculares (CNIC) under a 12h light/12h dark schedule (lights on at 7am, off at 7pm), with water and chow available ad libitum. Bmal1$^{\Delta N}$, CXCR4$^{\Delta N}$ and CXCR2$^{\Delta N}$ mutants in the C57BL/6 background have been described [14]. For the ALI experiments, Bmal1$^{\Delta N}$ and CXCR4$^{\Delta N}$ mice were backcrossed into the Balb/c background for at least 6 generations and we confirmed susceptibility to antibody-induced lung injury at this stage (not shown). All procedures with backcrossed mice were controlled using Cre-negative littermates. No specific randomization method was followed in this study. All experimental procedures were approved by the Animal Care and Ethics Committee of CNIC and the regional authorities.

Proteomic analysis of fresh and aged mouse neutrophils with ^{18}O

Neutrophils were obtained from the blood of C57BL6 mice using different strategies. For fresh neutrophils, mice were treated with AMD3100 (2.5 mg/kg i.p.) 1h before collection. For aged neutrophils, mice were treated with anti-P/E-selectin antibodies (1mg/kg i.v.) for 5d, every other day, before collection. Blood was obtained by collection in EDTA tubes to prevent coagulation. RBCs were precipitated using methylcellulose and leukocytes in the top phase were collected and washed before purification by negative selection. Negative selection was performed by incubation with biotinylated antibodies against CD3e, TER119, B220, CD8, CD115, CD4, CD49b and CD117, then incubated with streptavidin-coated beads and applied in a magnet for negative selection of neutrophils. We obtained neutrophils with a purity over 84%. 60 million neutrophils from each source were obtained for analysis.

For proteomic analyses, cell lysates were run on a SDS-PAGE gel (10% resolving gel and 4% stacking gel) at 50V. The electrophoresis was stopped when the front dye had barely passed into the resolving gel, ensuring concentration of all proteins into a unique band. Staining was performed using GelCode® Blue Stain (Thermo Scientific, San José, CA, USA). Gel pieces were cut into cubes (1 mm). For protein digestion, modified porcine trypsin (Promega) was added at a final ratio of 1:20 (trypsin-protein). Digestion proceeded overnight at 37ºC in 100 mM ammonium bicarbonate, pH 7.8. After in-gel trypsin digestion, the “fresh” samples were equally mixed with the “aged” samples which were labelled with 18O. The resulting tryptic peptide mixtures were subjected to nano-liquid chromatography coupled to mass spectrometry for

protein identification. Peptides were injected onto a C-18 reversed phase (RP) nano-column (75 µm I.D. and 50 cm, Acclaim PepMap100, Thermo Scientific) and analyzed in a continuous acetonitrile gradient consisting of 0-30% B in 240 min, 30-90% B in 3 min (B=90% acetonitrile, 0.5% acetic acid). A flow rate of ca. 200 nL/min was used to elute peptides from the RP nano-column to an emitter nanospray needle for real time ionization and peptide fragmentation on a Q-Exactive mass spectrometer (Thermo Fisher). An enhanced FT-resolution spectrum (resolution=70000) followed by the MS/MS spectra from most intense fifteen parent ions were analyzed along the chromatographic run (272 min). Dynamic exclusion was set at 30 s. For protein identification, tandem mass spectra were extracted and charge state deconvoluted by Proteome Discoverer 1.4.0.288 (Thermo Fisher). All MS/MS samples were analyzed using SEQUESTTM (Thermo Fisher). Sequest was searched with a fragment ion mass tolerance of 20 PPM and a parent ion tolerance of 15 PPM. Carbamidomethyl of cysteine was specified in Sequest as a fixed modification. Oxidation of methionine was specified in Sequest as a variable modification. Peptide quantification from FullScan spectra and labelling efficiency calculation were performed as described using QuiXoT, a custom software written in C#. Statistical analysis was done on the basis of a recently developed and validated random-effects model that includes four different sources of variance: at the spectrum-fitting, scan, peptide and protein levels 58. Briefly, the standardized variable Zq describes the log2 ratio for each protein corrected for the corresponding systematic error, in each experiment. Finally, data were plotted using R (v3.6.1 "*Action of the Toes*" making use of the libraries: *tidyverse, dplyr, DESeq2, ggplot2, ggrepel, ggpubr, clusterProfiler, biomaRt, DOSE, KEGG.db, org.Mm.eg.db, pheatmap, genefilter, RColorBrewer, GO.db, topGO, gage, ggsci, ReactomePA, gProfileR, varhandle, Hmisc, knitr, kableExtra, gghighlight, GSVA, msigdbr, enrichplot, gtools and VennDiagram*). The code will be provided upon request. Statistical data on all proteomics analysis are presented in **Supplementary Table 8**.

Proteomic analysis of human neutrophils by tandem mass tag (TMT)

For proteomic analysis of human neutrophils, two million isolated cells were pelleted in 1.5ml Eppendorf Tubes and snap-frozen at -80ºC. Upon analysis of purity, the best 5 samples (96 % mean purity) were used for multiplexed proteomic analysis at 8 am and 2 pm.

Total protein extracts from each sample were treated with 50 mM iodoacetamide (IAM) and digested overnight at 37°C with trypsin (Promega, Madison, WI, USA) at a 40:1 protein:trypsin (w/w) ratio using the Filter Aided Sample Preparation (FASP) digestion kit (Expedeon) according to manufacturer's instructions. The resulting peptides were desalted with C18 Oasis

cartridges (Waters Corporation, Milford, MA, USA), using 50% acetonitrile (ACN) (v/v) in 0.1% trifluoroacetic acid (v/v) as eluent, and vacuum-dried. The peptides were TMT-labeled following manufacturer's instructions, desalted, separated into 4 fractions using the high pH reversed-phase peptide fractionation kit (Thermo Fisher) and analyzed using a Proxeon Easy nano-flow HPLC system (Thermo Fisher, Bremen, Germany) coupled via a nanoelectrospray ion source (Thermo Fisher) to a Q Exactive HF Orbitrap mass spectrometer (Thermo Fisher). C18-based reverse phase separation was used with a 2-cm trap column and a 50-cm analytical column (EASY column, Thermo Fisher) in a continuous acetonitrile gradient consisting of 0-30% A for 240 min, 50-90% B for 3 min (A= 0.1% formic acid; B= 90% acetonitrile, 0.1% formic acid) at a flow rate of 200 nL/min. Mass spectra were acquired in a data-dependent manner, with an automatic switch between MS and MS/MS using a top 15 method. MS spectra in the Orbitrap analyzer were in a mass range of 400–1500 m/z and 120,000 resolution. HCD fragmentation was performed at 28 eV of normalized collision energy and MS/MS spectra were analyzed at 30,000 resolution in the Orbitrap.

All database searches were performed with Proteome Discoverer (version 2.1, Thermo Fisher) using SEQUEST-HT (Thermo Fisher) against a Uniprot database containing all sequences from Human (July, 2018; 20,408 entries). For database searching, parameters were selected as follows: trypsin digestion with 2 maximum missed cleavage sites, precursor mass tolerance of 2 Da, fragment mass tolerance of 30 ppm. Methionine oxidation (+15.994915) was set as a variable modification. Lysine and peptide N-terminal modification of + 229.162932 Da, as well as cysteine carbamidomethylation of +57.021464 Da, were set as fixed modifications. The same MS/MS spectra collections were also searched against inverted databases constructed from the same target databases. Peptide identification from MS/MS data was performed using the probability ratio method. False discovery rates (FDR) of peptide identifications were calculated using the refined method. A 1% FDR was used as the peptide identification criterion. Each peptide was assigned only to the best protein proposed by the Proteome Discoverer algorithm.

Quantitative information from TMT reporter intensities was integrated from the spectrum level to the peptide level, and then to the protein level based on the WSPP model (Navarro, P., et al 2014) using the Generic Integration Algorithm (GIA) (Garcia-marques, F- et al. 2016; Trevisan-Herraz, M. et al, 2018). Briefly, for the human experiment, for each sample i, the values $x_{qps} = \log_2 A_i/Ci$ were calculated, where A_i is the intensity of the TMT reporter of the 2pm sample from the individual i in the MS/MS spectrum s coming from peptide p and protein q, and Ci is the intensity of the TMT reporter from the 8am sample from the same individual.

Protein abundance changes are expressed in standardized units (z_q). Protein quantifications where further integrated among the 5 comparisons in the human experiment, obtaining for every protein averaged values (x_q') with their corresponding weights (w_q') (Navarro, P., et al 2014). The systems biology analysis was performed according to the SBT approach (Garcia-marques, F- et al. 2016). Significant abundance changes of proteins in the compared samples were detected at 1% FDR.

Data were analyzed using R (v3.6.1 "*Action of the Toes*" making use of the libraries: *tidyverse, dplyr, DESeq2, ggplot2, ggrepel, ggpubr, clusterProfiler, biomaRt, DOSE, KEGG.db, org.Hs.eg.db, pheatmap, genefilter, RColorBrewer, GO.db, topGO, gage, ggsci, ReactomePA, gProfileR, varhandle, Hmisc, knitr, kableExtra, gghighlight, GSVA, msigdbr, enrichplot, gtools and VennDiagram*). The analysis code will be provided upon request. Statistical data on all proteomics analysis is presented in **Supplementary Table 8**.

Proteomic analysis of mouse neutrophils by TMT

For proteomic analyses of mouse neutrophils, one hundred thousand cells were sorted from Bmal1$^{\Delta N}$ mice at ZT5 or ZT13 (see cell sorting section below). Total protein extracts were run on a SDS-PAGE gel (10% resolving gel and 4% stacking gel) at 50V, following the same protocol explained above in the 18O experiments. After the in-gel trypsin digestions the corresponding peptide mixtures were desalted with C18 Oasis cartridges and fractionated into 4 fractions according the methodology previously explained. All the fractions were subjected to liquid chromatography coupled to tandem mass spectrometry in a Q Exactive HF Orbitrap mass spectrometer using the same abovementioned method. TMT 10-plex isobaric reagents were used to label different replicates of neutrophil-derived peptide mixtures. Informatics and statistics analyses were performed using the same software above said.

Quantitative information from TMT reporter intensities was integrated from the spectrum level to the peptide level, and then to the protein level based on the WSPP model [58] using the Generic Integration Algorithm (GIA) [59, 60]. In the mouse TMT experiments, for each sample i, the values xqps= log2Ai/Ci were calculated, where Ai is the intensity of the TMT reporter from the individual *i* in the MS/MS spectrum *s* coming from peptide *p* and protein *q*, and Ci is the averaged intensity of the TMT reporters from all the samples in the given TMT experiment. The log2-ratio of each peptide (x_{qp}) was calculated as the weighted mean of its spectra, the protein values (x_q) were the weighted mean of its peptides, and the grand mean ($\bar{x}$) was calculated as the weighted mean of all the protein values (Navarro, P., et al 2014). The statistical weights of

spectra, peptides, and proteins (w_{qps}, w_{qp} and w_q, respectively) and the variances at each one of the three levels ($\sigma_{\mathbf{S}}^2$, $\sigma_{\mathbf{P}}^2$, and $\sigma_{\mathbf{Q}}^2$, respectively), were calculated as described [58]. Protein quantifications where further integrated among the corresponding replicates from the same condition, obtaining for every protein averaged values (x_q') with their corresponding weights (w_q') [58]. The systems biology analysis was performed according to the SBT approach (Garcia-marques, F- et al. 2016). Significant abundance changes of proteins in the compared samples were detected at 1% FDR.

Data were analyzed using R (v3.6.1 "*Action of the Toes*" making use of the libraries: *tidyverse, dplyr, DESeq2, ggplot2, ggrepel, ggpubr, clusterProfiler, biomaRt, DOSE, KEGG.db, org.Hs.eg.db, pheatmap, genefilter, RColorBrewer, GO.db, topGO, gage, ggsci, ReactomePA, gProfileR, varhandle, Hmisc, knitr, kableExtra, gghighlight, GSVA, msigdbr, enrichplot, gtools and VennDiagram*). The analysis code will be provided upon request. Statistical data on all proteomics analysis is presented in **Supplementary Table 8**.

Proteomics-transcriptomics correlations

To analyze the correlation between proteomics and transcriptomics data of fresh and aged neutrophils, we compared our proteomics data with previously-generated RNA sequencing data on fresh (sorted at ZT13 from blood) and aged neutrophils (sorted at ZT5 from blood) available in GEO: GSE86619 [14]. To this end we obtained a set of common proteins and genes from both datasets, compared the proteomics Z-score and the sequencing Log2FC (both inform about the relative enrichment in fresh neutrophils) and calculated the regression statistics using R (v3.6.1 "*Action of the Toes*"). We performed similar correlation analyses for paired transcriptome and proteome data from human samples.

Cytometry and cell sorting

Cytometric analyses were performed using a Sony SP6800 Spectral Analyzer (Sony Biotechnology, Japan). Analysis was performed using Flowjo vX (Tree Star Inc, Ashland, OR). Cell sorting experiments were performed using an FACS Aria cell sorter (BD Biosciences). All analyses were conducted at the Cellomics Unit of the CNIC. The following antibodies and streptavidin conjugates were used in this study:

Antibody /	Clone	Species	Manufacturer
CD16-APC	3G8	Human	BD
CD62L-FITC	DREG56	Human	BD
CD11b-PE	M1/70	Human/Mouse	Tonbo biosciences
Ly6G-AF647	1A8	Mouse	eBioscience

CD45-APC/Cy7	104	Mouse	Biolegend
CXCR2-PerCP-Cy5.5	SA044G4	Mouse	Biolegend
CXCR4-PE	2B11	Mouse	eBioscience
CD41-PE	MWReg30	Mouse	eBioscience
CD62L-FITC	MEL-14	Mouse	eBioscience
CD11b-BV510	M1/70	Mouse	Biolegend
CD31-APC	390	Mouse	eBioscience
CD31	2H8	Human/Mouse	Thermo Fisher
MPO-biotin	Polyclonal	Human/Mouse	R&D (biotinylated in-house)
citH3 (R2+R8+R17)	Polyclonal	Human/Mouse	Abcam
Goat-anti-hamster-AF405	Polyclonal	Hamster	Jackson ImmunoResearch
Goat-anti-rabbit-AF647	Polyclonal	Rabbit	Thermo Fisher
Streptavidin-AF488	N/A	Mouse/Human/Rat	BioLegend

In vivo NET formation during ischemia/reperfusion

The cremaster muscle was exteriorized as reported [14], and ischemia was achieved by occlusion of the inflowing and outflowing vessels by clamping the tissue connecting the muscle and the animal's body with a 15mm Micro Serrefine clamp (Fine Science Tools, Heidelberg, Germany) for 45 min. Reperfusion was achieved by removal of the clamp. 15 min after reperfusion, mice were euthanized and cremasters muscle removed for analysis. Excised cremaster muscles were fixed in 4% paraformaldehyde at 4ºC overnight and then washed 3 times in PBS containing 0.5% Triton-x 100 (PBST) and blocked for 2 h in PBST 25% FBS at room temperature with shaking. Staining was performed using anti citrunillated-H3, anti-MPO and anti-CD31 antibodies in 10% FBS-PBST overnight at 4ºC with shaking. Then, secondary antibodies were stained in 10%FBS-PBST for 4h at room temperature. Samples were then washed and mounted in Mowiol 4-88 (Mw 31,000; Sigma). Imaging of whole-mount cremaster muscles was performed using a Nikon A1R confocal system coupled to a Nikon Eclipse-Ti inverted microscope with the following lines: Diode 402nm Argon Laser 457, 476, 488, 514nm Diode 561nm HeNe Laser 642nm using a Plan Apo 10x/0,45 dry objective and the software NIS Elements AR 4.30.02 (Build 1053 LO, 64 bits, Nikon Instruments, Tokyo, Japan) for acquisition of confocal 3D tile-scan images of the whole cremaster muscle, which were afterwards analyzed using Imaris (Bitplane AG, Zurich, Switzerland). All imaging was performed at the Microscopy & Dynamic Imaging Unit of CNIC.

Quantification of primary granules

Blood samples were extracted every 4 h during 24 h from wild-type mice, starting at ZT1 (corresponding to 8 am). 100 microliters of blood were RBC-lysed in hypotonic lysis buffer

(0.15M KH4Cl, 0.01M KHCO3 and 0.01M EDTA in water), washed with PBS and resuspended in 40 microliters of PBS. Smears were then performed onto Superfrost Plus microscope slides (Thermo Scientific, Waltham, USA) and cells were immediately fixed in 4% PFA for 10 min at room temperature. For the experiments with mutant mice, neutrophils were sorted as described, cytospun (600 RPM, medium acceleration) into microscope slides and fixed with PFA 4% for 10 min at room temperature. For CXCL2 stimulation experiments, sorted neutrophils were plated with RPMI medium on Poly-L-lysine covered 8-well µ-Slides (Ibidi, Martinsried, Germany) and left 30 min to adhere. Cells were then incubated for 1h with 50ng/ml of recombinant CXCL2 (R&D Systems) or vehicle, and fixed with 4% PFA in PBS.

For neutrophils in blood vs tissues, we sorted cells and cytospun them as described. Prior to sorting, the tissues were extracted and kept in cold PBS (except liver, kept at room temperature in HBSS) and processed immediately after. To avoid activation of neutrophils, we did not perform digestion of the tissues, but mechanically dissociated them into single-cell suspensions by straining in 100µm pore cell strainers (Falcon). Enrichment of leukocytes from liver was performed by 36% Percoll (GE Healthcare) in HBSS (Invitrogen) gradient centrifugation. Single-cell suspensions were incubated with antibodies against CD45 (eBiosciences), CD11b (Biolegend) and Ly6G (BioXcell) prior to sorting of CD45+, CD11b+, Ly6G+ neutrophils. Finally, cytospun neutrophil were fixed for 10 min in PBS containing 4% PFA.

For the light cycle inversion experiments, WT mice were housed in light cabinets with inverted light cycle for three weeks prior to blood withdrawal for analysis. Then, whole blood extracted in EDTA tubes was RBC-lysed and smears were performed as described above.

In all cases, after washing, cells were permeabilized for 30 min with 0.1% Triton, 25% FBS in PBS and stained with biotinylated anti-MPO antibody (R&D Sytems) at 4ºC overnight. Afterwards, cells were washed and incubated with A488-conjugated Streptavidin for 3h at room temperature. Finally, cells were washed, stained with DAPI and mounted in Mowiol. Imaging was performed using a Leica SP8 X confocal microscopy system coupled to a DMI6000 inverted microscope, with 100x (HC PL Apo CS2 100x/1.4 OIL) magnification objective. Granule contents were analyzed using the Imaris software.

Ex vivo NET-formation assays

Neutrophils were sorted as previously described and $5x10^4$ neutrophils were plated with RPMI medium on Poly-L-lysine covered 8-well µ-Slides (Ibidi, Martinsried, Germany), and left 30 min to adhere. Subsequently, cells were incubated for 2h with 100nM PMA or vehicle. Cells were

then fixed using PFA 4% for 10 min, permeabilized with PBS 0.1% Triton X-100 1% goat serum plus 5% BSA and stained with antibodies against citrullinated histone 3 (Abcam, Cambridge, UK), DNA (Sytox green, Molecular Probes) and MPO (R&D Systems). Whole-slide z-stack tilescan images were acquired with a Nikon A1R confocal system coupled to a Nikon Eclipse-Ti inverted microscope or a Leica SP5 confocal microscope and analysed using Imaris.

Antibody-induced acute lung injury (ALI)

A two-event model of transfusion-related ALI was adopted for our studies as described [17]. Male Balb/c mice (7-14 week-old) were injected intraperitoneally with 0.1 mg/kg LPS. 24 hours later, mice received an intravenous injection of 0.5 mg/kg anti-H2d (clone 34-1-2s; BioXcell) antibody. Some mice were treated 1h before ALI induction with 12mg/kg of Cl-Amidine (Cayman Chemical Company, Ann Arbor, Michigan, USA) to block NET-formation (31). For survival experiments, mice were observed for 2h during the acute phase of ALI.

Neutrophil elastase activity assay

NE activity in plasma was measured using a commercially available kit (Neutrophil Elastase activity assay kit - Fluorometric, NAK246-1KT, Sigma-Aldrich) according to the manufacturer's instructions. We analyzed 50 microliters of plasma, with an excitation wavelength of 390nm and emission wavelength of 510nm in a Fluoroskan Ascent plate reader (Thermo Labsystems). Standard curve goodness of fit had an R-square of 0.99 in linear regression.

Intravital imaging of the lung

Intravital microscopy of the lung was performed as reported [33]. Briefly, mice were anesthetized and mechanically ventilated through the trachea using a small animal ventilator model 687 (Harvard Apparatus). Then, right lateral thoracotomy was applied, and the lung was positioned under the window of a custom-built fixation device. A mil vacuum was applied to hold the lung in position during microscopy. Mice were injected with AF647-conjugated Ly6G antibody (clone 1A8; BioXcell) to stain neutrophils, PE-conjugated CD41 antibody (eBioscience) to stain platelets and Sytox green (Molecular Probes) to stain extracellular DNA. 4D imaging was performed for each mouse in 5 random fields inside the visualization window, using the VIVO system built by 3i (Intelligent Imaging Innovations, Dever, CO) upon an Axio Examiner Z.1 workstation (Zeiss, Oberkochen, Germany) and mounted on a 3D motorized stage (Sutter Instrument, Novato, CA). The system was equipped with a CoolLED pE widefield fluorescence LED light source (CoolLED Ltd. UK) and a quad pass filter cube with Semrock Di01-R405/488/561/635 dichroic and FF01-446/523/600/677 emitter. A plan-apochromat 20x W NA1.0 objective (Zeiss) was used. For confocal IVM, we used laser stacks for 488, 561 and

640nm beams coupled with a confocal scanner (Yokogawa CSUX-A1; Yokogawa, Japan) and images were acquired with 3µm Z and 15 seconds intervals. The system was run on a Dell Precision T7500 computer system (Dell Inc., Round Rock, TX) using the SlideBook software (Intelligent Imaging Innovations). Analysis was performed in Imaris software. For NET-like structures, we quantified the number of spots in the neutrophil-extracellular DNA colocalization channel over time in all random fields.

Analysis of NET types in lungs

We found two types of NET-formation events in lungs during ALI. Flowing NETs were defined as events in which DNA was rapidly extruded out of the neutrophil and most commonly was washed away by the flow; and adherent NETs, which were defined as DNA being deployed slowly around the uropod region of the neutrophil as it crawled, stuck to the vasculature and was more resistant to blood-flow washing. To quantify the relative frequency of each of them, we visually inspected every NET formation event in our time-lapse footage and ascribed each event to one of the two categories, or none if it was unclear.

Whole mount immunostaining and tissue clearing

To confirm the presence and abundance of NETs in the lungs of mice upon ALI induction we performed whole mount immunostaining and tissue clearing of excised lungs. Mice were subject to ALI and euthanized with CO_2 15 min after ALI induction. Mice were then perfused with 20ml of saline through the left ventricle of the heart, and the lungs were collected in cold PBS. Afterwards, lungs were fixed at 4ºC overnight in PBS with 4% PFA and 30% sucrose. After 3 washes of 1h with PBS at room temperature, tissues were permeabilized in methanol gradients in PBS for 30 min (PBS > MetOH 50% > MetOH 80% > MetOH 100%). Then, tissues were bleached with Dent's bleach (15% H_2O_2, 16.7% DMSO in MetOH) for 1h at room temperature, and then were rehydrated through descending methanol gradients in PBS (MetOH 80% > MetOH 50% > PBS). Then tissues were incubated with blocking buffer containing PBS with 0.3% Triton X100, 0.2% BSA, 5% DMSO, 0.1% azide and 25% FBS overnight at 4ºC with shaking. Afterwards lungs were stained with antibodies against citrunillated histone 3 (rabbit, Anti-Histone H3 —citrulline R2 + R8 + R17— antibody, Abcam), MPO (Human/Mouse Myeloperoxidase/MPO Antibody, R&D biotinylated in house) and CD31 (CD31 Monoclonal Antibody –2H8–, Thermo Fisher) for 2 days at 4ºC with shaking. After washing for 24h in washing buffer (PBS with 0.2% Triton X100 and 3% NaCl), the tissues were stained with secondary antibodies anti-rabbit AF647, antiHamster-AF405 and Streptavidin AF488 for 24h at 4ºC with shaking. 24h later, tissues were washed for 24h in washing buffer and were

dehydrated in MetOH gradients in dH_20 using glass containers for 30 min in each step (MetOH 50% > MetOH 70% > MetOH 90% > 3x MetOH 100%). Finally, tissues were cleared for 30 min in MetOH with 50% BABB and afterwards in 100% BABB (benzyl alcohol, benzyl benzoate 1:2) and imaged in a Leica SP8 X confocal microscopy system coupled to a DMI6000 inverted microscope.

Computerized tomography (CT) for in vivo edema quantification

In vivo CT imaging was performed on a nanoPET/CT small-animal imaging system (Bioscan, Washington DC) equipped with a micro-focus X-ray source and a high-resolution detector (1024x3596 pixels; 48 μm pixel size). Acquisition parameters were 55 kVp and 73 μAs. Mice were intraperitoneally anesthetized and positioned onto a thermoregulated (30 degrees) mouse bed until the scan was completed. An ophthalmic gel was administered in their eyes to prevent retinal drying. Six studies were acquired per animal: one prior the retro-orbital injection of anti-H2d to induce ALI, and five post-injection during 30 min approximately. Data were acquired in helical mode obtaining 240 projections per rotation with 768 μm pixel size. Reconstruction was performed with an FDK-based method included in the proprietary Nucline software (Mediso, Budapest, Hungary). Pulmonary edema was quantified using Horos software (The Horos Project, distributed under the LGPL license at Horosproject.org and sponsored by Nimble Co LLC d/b/a Purview in Annapolis, MD, USA) as the change of the mean value, in Hounsfield Units, within the region of interest of the lungs obtained by thresholding (-1000 and -400 lower and upper thresholds, respectively) followed by a closing morphological operation.

Intravital imaging of the cremaster muscle to quantify platelet-neutrophil interactions

Intravital microscopy of the cremaster muscle after TNFα stimulation (R&D Systems, 0.5μg intrascrotal injection) was performed as previously reported [14, 17] using the VIVO system. Ten to twenty venules segments per mouse were analyzed 150 to 210 min after TNF-α treatment in multiple fluorescence channels (Cy3/561 for PE, FITC/488 for FITC and Cy5/640 for APC) and bright-field images with 1x1 or 2×2 binning with 3 second interval for 2 min on each field of view. For double staining with PE- and FITC-conjugated antibodies, acquisition was facilitated in single (FITC) and quadrant (PE) filters in order to avoid bleed-through of fluorescent signals between channels. For the visualization of leukocytes, fluorescently labelled anti-Ly6G-APC and anti-CD62L-FITC antibodies were injected, and to visualize platelets, anti-CD41-PE was injected intravenously at 1 μg/mouse. Quantification of neutrophil-platelet interactions in either the leading edge or trailing edge was performed using Slidebook.

Circadian analysis of neutrophil phenotypes

Circadian blood samples were extracted every 4 h during 24 h from wild-type or experimental mice, starting at ZT1 (Zeitgeber time, 1 hour after the onset of light, 7:00 at the CNIC's animal facility). For circadian surface marker analysis, Blood counts were analyzed in an automated hemocytometer (Abacus Junior, Diatron; Holliston, USA)RBC were lysed in hypotonic lysis buffer (0.15M KH4Cl, 0.01M KHCO3 and 0.01M EDTA in water) and incubated 15 min with 0.25 µg anti-Ly6G (1A8 clone, BioXcell), -CD62L (Biolegend) and -CXCR2 (eBioscience) antibodies, washed and analysed in a Sony SP6800 Spectral Analyzer. Analysis was performed using Flowjo vX (Tree Star Inc, Ashland, OR).

Vascular permeability assay

A 0.5% solution of Evans blue in sterile PBS was prepared and 200µl of the solution was i.v. injected into mice 15 min before TRALI induction (or just LPS injection as control, see protocol for ALI). 15 min later mice were sacrificed and tissues extracted and weighted. Then, tissues were submerged in 0.5 ml formamide and incubated at 55ºC for 24h. Tissues were removed, and the tubes centrifuged for 5 min at 645 g. Finally, supernatants were measured for absorbance at 610nm using an xMark Microplate Spectrophotometer (BioRad) plate reader.

Human studies

We performed human proteomics, RNA sequencing, NET-formation assays and granule quantification (see individual methods) in neutrophils from blood samples of heathy volunteers obtained at 8am, 2pm and 7pm at Hospital 12 de Octubre. The study complied with all ethical regulations and was approved by the Ethical Research Committee of Hospital 12 de Octubre in Madrid (CEIm #18/389), and informed consent was obtained from all volunteers.

Human neutrophil granule quantification

Diurnal blood samples were extracted from healthy volunteers at 8am, 2pm and 7pm. One hundred microliters of blood were RBC lysed in hypotonic lysis buffer (0.15M KH4Cl, 0.01M KHCO3 and 0.01M EDTA in water), washed with PBS and resuspended in 40 microliters of PBS. Cells were processed as imaged as indicated above for mouse neutrophils.

Human neutrophil isolation

12 ml of freshly obtained blood extracted from healthy volunteers at the indicated times were used to isolate human neutrophils using Histopaque 1119 and 1077 (Sigma) gradients. In a 50ml falcon tube 15ml of Histopaque 1119 were added and then 15 ml of Histopaque 1077 were

carefully layered on top. Whole blood was carefully layered on top of the low density solution, and tubes were centrifuged for 30 min at 340g at room temperature, with no brakes or acceleration. Neutrophils layering between the 1077 and 1119 interphase were carefully aspirated and the isolated neutrophils washed twice in PBS. We obtained over 95% purity as assessed by flow cytometry.

RNA sequencing of human neutrophils

Total RNA was prepared with the RNA Extraction RNeasy Plus Mini-kit (QIAGEN). 1 ng of total RNA were used to generate barcoded RNA-seq libraries using the NEBNext Single Cell/Low Input RNA Library Prep Kit for Illumina (New England Biolabs) according to manufacturer's instructions. First cDNA strand synthesis were performed and then amplified by PCR followed by fragmentation. Next, cDNA ends were repaired and adenylated. The NEBNext adaptor was then ligated followed by second strand removal, uracile excision from the adaptor and PCR amplification. The size of the libraries was checked using the Agilent 2100 Bioanalyzer and the concentration was determined using the Qubit® fluorometer (Life Technologies)

Libraries were sequenced on a HiSeq2500 (Illumina) to generate 60 bases single reads. FastQ files for each sample were obtained using *bcl2fastq* 2.20 Software software (Illumina). The RNA sequencing experiments were performed at the Genomics Unit at CNIC.

Human ex vivo NET formation assay

$4x10^4$ Human neutrophils isolated as previously described were plated with RPMI medium on Poly-L-lysine covered 8-well µ-Slides (Ibidi, Martinsried, Germany) and left 30 min to adhere. Adherent cells were incubated for 2h with 250ng/ml PMA or vehicle and then fixed using PFA 4% for 10 min, permeabilized with PBS 0.1% Triton X-100 1% goat serum plus 5% BSA and stained with antibodies against citrullinated histone 3 (Abcam, Cambridge, UK), DNA (Sytox green, Molecular Probes) and MPO (R&D Systems). Whole-slide z-stack tilescan images were acquired with a Leica SP5 confocal microscope. Analysis of extra-nuclear DNA was performed using ImageJ with an automated method for extranuclear DNA quantification made available in https://doi.org/10.6084/m9.figshare.7358642.v1

Retrospective analysis of human ARDS

Data from acute respiratory distress syndrome (ARDS) was extracted from a prospective observational cohort study of 5334 consecutive adult patients with community-acquired pneumonia admitted to the ICU that developed ARDS between 1996 and 2016 [38], in Hospital Clinic of Barcelona, Spain. The time of admission, severity and survival was determined for the

125 patients that developed ARDS. Patients were excluded if they had severe immunosuppression or active tuberculosis. ARDS was identified based on the Berlin definition. Only time points with 3 or more data points were included in subsequent analysis. The study was approved by the ethics committee of Hospital Clinic of Barcelona (no. 2009/5451).

Transmission electron microscopy imaging of neutrophils

Neutrophils from mouse and human blood were isolated as previously described (FACS sorting for mouse neutrophils, gradient isolation for human neutrophils), fixed in 4% PFA for 10 min and washed with PBS. Samples were then post-fixed in distilled water containing 4% of osmium tetroxide for 1h at room temperature. After washing in distilled water, samples were stained in a block with uranyl acetate 0.5% in water for 10 min. Then, samples were dehydrated in ascending gradients of ethanol in water (30%, 50%, 70%, 95% and 100%) with a last step in acetone. Samples were then included in epoxi resin (Durcupan) in ascending steps of resin:acetone (1:3, 3:1) and then pure resin. Samples included in the resin were polymerized for 48h at 60ºC and 60nm slices were obtained in a Leica Ultracut S ultramicrotome in 200 mesh Cu gratings. Finally, samples were counterstained with uranyl acetate and lead citrate. Images were acquired in a 100Kv Jeol JEM1010 TEM microscope (Tokyo) with a Gatan SC200 (Pleasanton CA) camera coupled to the system. Quantification of granule-covered cytoplasmic area was performed in ImageJ using a custom-made macro that allows calculation of cell, nucleus and granule areas, made available in: https://doi.org/10.6084/m9.figshare.7619093.v1

Data availability

Proteomics data for mouse and human neutrophils are available in the Peptide Atlas with accession number: PASS01364 (for reviewers, use dataset password NG2939hf). Proteomics data for Bmal1$^{\Delta N}$ mice at ZT5 and ZT13 and WT vehicle vs AMD-3100 treated mice are also available in the Peptide Atlas with the accession number: PASS01438 (for reviewers, use password WD4442nbw). Mouse circadian transcriptomics used for the correlation analysis are available at the Gene Expression Omnibus with accession number GSE102310. Human sequencing data used for the correlation analysis are available at GEO with accession number: GSE136632 (for reviewers, use password sjotiiailxcfvgd). All other pieces of data are available upon request.

Code availability

ImageJ macros for TEM granule quantification and extracellular DNA quantification are available in FigShare (see the relevant method for specific links). All other pieces of code are available upon request.

Statistical analysis

Unless otherwise indicated, data are represented as mean values ± standard error of the mean (SEM). Paired or unpaired t-test was used when 2 groups were compared, and comparison of more than two data sets was done using one-way analysis of variance (ANOVA) with Turkey's post-test. Where applicable, normality was estimated using D'Agostino & Pearson or Shapiro-Wilk normality test. Log-rank analysis was used for Kaplan-Meier survival curves. Sample exclusion was not performed unless evident signs of disease were found in a mouse. For determination of diurnal patterns, we performed COSINOR fitting of circadian curves, using the curve-fitting module of Graphpad Prism (v7) with the equation Y = Baseline + Amplitude x cos (Frecuency X + Phaseshift), where Baseline = average of Ymax and Ymin; Amplitude = 0.5 x (Ymax - Ymin), where Frecuency=0.2618 and Phaseshift= value of X at Ymax. To determine whether a diurnal curve displayed an oscillating pattern we used the COSINOR-calculated amplitudes and compared them with a hypothetical zero-amplitude curve (i.e. with no circadian behavior) assuming that both curves have identical standard deviations. We finally compared the two curves' amplitudes using unpaired t-test analyses. All statistical analyses were performed using Prism v7 (GraphPad Software, California, USA), except proteomics and sequencing analysis, which were performed using R (see individual methods). A p-value below 0.05 was considered statistically significant; non-significant differences (n.s.) are indicated accordingly.